REPORT DOCUMENTATION PAGE

Form Approved
OMB No. 0704-0188

1. AGENCY USE ONLY (Leave blank)	2. REPORT DATE	3. REPORT TYPE AND DATES COVERED
	1/13/1997	Final 15 Jan. 1990 - 31 Dec. 1995

4. TITLE AND SUBTITLE

Fine-Scale, Near Bottom Geological and Geophysical Studies of Ocean Crust in the ONR-ARSRP Acoustic Reverberation Corridor See Title Page

5. FUNDING NUMBERS

G N00014-90-J-1621

6. AUTHOR(S)

Brian E. Tucholke, Gary Jaroslow, W. Kenneth Stewart and Martin C. Kleinrock

7. PERFORMING ORGANIZATION NAME(S) AND ADDRESS(ES)

Woods Hole Oceanographic Institution
Woods Hole, MA 02543

8. PERFORMING ORGANIZATION REPORT NUMBER

131621SP

9. SPONSORING/MONITORING AGENCY NAME(S) AND ADDRESS(ES)

Office of Naval Research
800 North Quincy Street
Arlington, VA 22217

10. SPONSORING/MONITORING AGENCY REPORT NUMBER

11. SUPPLEMENTARY NOTES

12a. DISTRIBUTION/AVAILABILITY STATEMENT

Approved for public release; distribution is unlimited.

12b. DISTRIBUTION CODE

13. ABSTRACT *(Maximum 200 words)*

The Acoustic Reverberation Special Research Program required detailed knowledge of large- and small-scale seafloor roughness, crustal structure, sediment-distribution patterns, and material properties of the ocean floor on the Mid-Atlantic Ridge in order to advance fundamental research on acoustic-wave scattering from the ocean bottom and subbottom at low frequencies and over long propagation paths. To provide this information and to improve our understanding of the fundamental geological processes that control formation and evolution of ocean crust and deposition of the overlying sediments, we conducted two geological/geophysical surveys in the Acoustic Reverberation Corridor within the ONR Atlantic Natural Laboratory at 25°25' to 27°10'N, 45°00' to 49°00'W. The initial survey acquired regional geological and geophysics data, and the second survey acquired fine-scale, near-bottom data at four seafloor sites identified by ARSRP researchers as prime acoustic study areas. This report summarizes the results of our geological and geophysical research on ridge-flank tectonic segmentation; the structure, roughness, composition, thickness and magnetization of the ocean crust; gravity anomalies; sediment distribution; fault patterns and fault-scarp denudation; and seamount construction and degradation.

14. SUBJECT TERMS	15. NUMBER OF PAGES
Mid-Atlantic Ridge, acoustic reverberation, crustal structure, crustal magnetization, sediment distribution, faults, abyssal hills, topography, gravity, seamounts, mass wasting	45
	16. PRICE CODE

17. SECURITY CLASSIFICATION OF REPORT	18. SECURITY CLASSIFICATION OF THIS PAGE	19. SECURITY CLASSIFICATION OF ABSTRACT	20. LIMITATION OF ABSTRACT
Unclassified	Unclassified	Unclassified	

NSN 7540-01-280-5500

DTIC QUALITY INSPECTED 1

Standard Form 298 (Rev. 2-89)
Prescribed by ANSI Std. Z39-18
298-102

MORPHOLOGICAL AND GEOPHYSICAL INVESTIGATION OF WESTERN NORTH ATLANTIC OCEAN CRUSTAL STRUCTURE: ENVIRONMENTAL WORK IN SUPPORT OF THE ACOUSTIC REVERBERATION SPECIAL RESEARCH PROGRAM

and

MORPHOLOGICAL AND GEOPHYSICAL INVESTIGATION OF WESTERN NORTH ATLANTIC OCEAN CRUSTAL STRUCTURE

and

FINE-SCALE, NEAR-BOTTOM GEOLOGICAL AND GEOPHYSICAL STUDIES OF OCEAN CRUST IN THE ONR-ARSRP ACOUSTIC REVERBERATION CORRIDOR

Final Report for ONR Grant N00014-90-J-1621

Brian E. Tucholke, Gary E. Jaroslow and W. Kenneth Stewart
Woods Hole Oceanographic Institution, Woods Hole, MA 02543
Email: btucholke@whoi.edu, gjaroslow@whoi.edu, kstewart@whoi.edu
Ph. (508) 457-2994, (508) 457-2491, (508) 457-2644
FAX (508) 457-2187, (508) 457-2187, (508) 457-2191

Martin C. Kleinrock, Vanderbilt University, Nashville, TN 37235
Email: kleinrmc@ctrvax.vanderbilt.edu
Ph. (615) 322-2420
Fax (615) 322-2138

LONG-TERM GOALS

Our long-term goals are: 1) To develop geological models that explain the origin and distribution of morphological and compositional features of the ocean crust and sedimentary record, and that predict these features in unsurveyed or poorly surveyed areas. 2) To provide geological and geophysical data and models to the acoustics research community and to work with them on interpretation of seafloor geology to enhance our understanding of bottom/subbottom reverberation in the ocean basins.

BACKGROUND AND OBJECTIVES

The Acoustic Reverberation Special Research Program (ARSRP) required detailed knowledge of both large- and small-scale seafloor roughness, sediment-distribution patterns, and material properties in order to advance fundamental understanding of acoustic-wave scattering from the ocean bottom and subbottom at low frequencies and over long propagation paths. To provide this information and to improve our understanding of the fundamental geological processes that control formation and evolution of ocean crust and sedimentary patterns, we conducted two geological/geophysical surveys in the

Acoustic Reverberation Corridor within the ONR Atlantic Natural Laboratory (25°25'N - 27°10'N, 45°00'W - 49°00'W). We initially conducted a regional survey in 1992 (R/V Ewing Cruise 9208), acquiring seafloor-backscatter imagery (HMR1 long-range sidescan sonar), Hydrosweep multibeam bathymetry, gravity, magnetics, and single-channel seismic and 3.5-kHz reflection data. In 1993, we conducted fine-scale, near-bottom surveys (R/V Knorr Cruise 138-14) to study the detailed geology and geophysics of four seafloor sites identified by ARSRP researchers as prime targets within the Acoustic Reverberation Corridor; survey instrumentation included the DSL-120 bathymetric sonar and the Remotely Operated Vehicle (ROV) Jason. We collected precisely navigated deep-towed sidescan sonar and phase-difference bathymetry (120 kHz, 200 kHz); forward-scan sonar (300 kHz); precision pencil-beam (Mesotech) bathymetry; magnetics; video, film, and electronic still photography; and seafloor rock samples (ROV Jason sampling, and dredging). During 1995-1996 we analyzed the regional survey data and we also analyzed subsets of the fine-scale survey data that were processed with available funding.

The data from our surveys and our geological interpretations were made available to ARSRP researchers, and they have also been presented to the broader research community in the form of both oral presentations and papers in scientific journals. The Bibliography at the end of this report summarizes our contributions. The principal results of our research are summarized below.

RESULTS

Ridge-Flank Segmentation and Crustal Structure

Our regional geological/geophysical survey of the western flank of the Mid-Atlantic Ridge extended from 25° 25' N to 27° 10' N and from the ridge axis out to 29 Ma crust (Figures 1 and 2; Tucholke et al., in press, b). The survey covered all or part of nine spreading segments, all bounded by non-transform, mostly right-stepping discontinuities which are subparallel to flowlines but which migrated independently of one another (Figure 3). Some discontinuities alternated between small right- and left-stepping offsets or exhibited zero offset for up to 3-4 m.y. Despite these changes in discontinuities, the spreading segments have been long-lived, extending up to 20 m.y. across isochrons.

A large change (~9°) in relative plate motion occurred about 24-22 Ma (Figure 3), resulting in a plate-boundary reorganization that included both elimination of segments and generation of new segments. The nature of this plate-boundary response, and the persistence of segments through periods where their bounding discontinuities had zero offset, suggest that the position and longevity of segments is controlled primarily by the subaxial position of buoyant mantle diapirs or focussed zones of rising melt.

Along the full cross-isochron run of each segment, there are distinct differences in seafloor depth, crustal structure and thickness, and bulk lithosphere composition between inside corners (formed in the bight between the spreading axis and the active offset), segment centers, and outside corners (formed adjacent to the inactive trace of the offset). This demands a fundamentally asymmetric process of crustal accretion and extension across the ridge axis, and we attribute this structure to the occurrence of low-angle normal (detachment) faulting toward segment ends (Tucholke and Lin, 1994). Inside corner crust comprises the footwall of the detachment fault, and outside-corner crust forms the hanging wall. The volcanic upper crust is typically contained within the hanging wall, and it is stripped from the inside-corner footwall and transported to the outside-corner part of a spreading segment.

Detachment faulting creates thin crust in inside-corner regions of spreading segments adjacent to both transform and non-transform offsets (Tucholke et al., 1996b). Large, elongate to quasi-circular domes (megamullions) are common inside-corner morphological features, and they typically are 0.5-1.5 km high and 5-15 km in diameter. Megamullions have strongly positive residual gravity anomalies and thus apparently very thin crust, as is locally confirmed by dredging of gabbros and peridotites (Figure 4). The features are analogous to "turtleback" metamorphic core complexes formed by detachment faulting in subaerial extensional environments (Figure 4). The similarities of the submarine and subaerial megamullions suggest that geological relationships observed in metamorphic core complexes on land can yield significant insights into the structure and origin of the domes developed in slow-spreading ocean crust.

Our studies show that the surface of many of the oceanic megamullions appears to be an exposed low-angle fault. The fault dips gently toward the spreading axis on the axial (down-dip) side of the megamullion, and away from the axis on the opposite, up-dip side, much as would be expected from development of a "rolling hinge". Smaller-scale, extension-parallel mullions corrugate the fault surface, and they exhibit two kinds of character. Low-amplitude mullions are sinusoidal in the direction of fault strike, and they have amplitudes of a few tens of meters and wavelengths up to several hundred meters. High-amplitude mullions are up to 600-900 m high, 6-8 km wide, and tend to be more isolated and peaked in cross-section. Overall, mullion amplitudes average about 5% of mullion wavelength at all scales. The occurrence of mullioned fault surfaces supports the concept that low-angle detachment faults develop at the ends of segments in slow-spreading environments; the extent of the faults in the dip direction indicates that the faults are active for periods up to 1-2 m.y.

Over the cross-isochron run of segments, variations in residual mantle Bouguer gravity (Figure 5) suggest cyclic, 2-3 m.y. changes of at least 1-2 km in crustal thickness. These are interpreted to be caused by episodes of magmatic versus relatively amagmatic extension, controlled by retention and quasi-periodic release of melt from the upwelling mantle. Detachment faulting appears to be especially effective in exhuming lower crust to upper mantle at inside corners during the relatively amagmatic episodes, creating the dome-like megamullions.

Magnetization of Slow-Spreading Ocean Crust

Our detailed sea-surface magnetic data over the west flank of the Mid-Atlantic Ridge, acquired during Ewing Cruise 9208, documented the history and evolution of crustal magnetization in slowly accreted crust (Figure 3; Tivey and Tucholke, 1996, submitted). We compared crustal magnetization against tectonic province and found no difference between inside- and outside corner crust, indicating that the off-axis magnetic signal is not sensitive to crustal architecture or lithology. This implies that the contribution of extrusive volcanic rocks to the anomaly pattern is not significant at ridge-segment ends.

We also investigated off-axis crustal magnetization and found that while normally magnetized crust shows little or no variation along isochrons, reversely magnetized crust shows significantly more positive magnetization towards segment ends. We attribute this trend to the preferential destruction of original remnant magnetization at segment ends and the substitution of either viscous or induced magnetization. Such magnetization is always positive for a normal-polarity period and will tend to maintain the linearity of magnetic anomalies if they are subparallel to the spreading ridge and magnetic meridian, which is the case for the Mid-Atlantic Ridge. These observations, along with the finding that the presence or absence of extrusive crust has little effect upon the magnetic signal, suggest that the source of this additional magnetization lies within lower-crustal gabbros or upper-mantle peridotites.

Finally, from an analysis of magnetization decay with age it is apparent that while a decrease over the first 10 m.y. is present, a faster decay cannot be unambiguously resolved by sea-surface magnetic data. At slow spreading rates, the aliasing created by the crustal accretion process, by finite anomaly transition widths, and by the inherent filtering of water depth produce an *apparent* rapid decay over the first 5 m.y. Our study does not preclude such a fast decay rate, but it suggests that only near-bottom surveys with increased resolution are able to properly resolve such decay trends.

Sediment Distribution Patterns on the Ridge Flank

Sediment thickness was mapped from a combination of seismic-reflection profiles, multibeam bathymetry, and sidescan-sonar imagery (Jaroslow, 1997). The primary seismic (watergun) data were obtained during Ewing Cruise 9208, and these data were supplemented by other, earlier Lamont-Doherty Earth Observatory seismic profiles (airgun), and by a single near-bottom profile obtained by the Naval Research Laboratory (NRL) DTAGS system across a large sediment pond located at 26°10'N, 46°15'W. Picks of sediment thickness in reflection time were made ~0.5 km apart along ship tracks, and the spacing between ship track lines was 4 to 9 km. To contour sediment thickness, trends were interpolated following the structure observed in Hydrosweep multibeam bathymetry. We also used HMR1 long-range sidescan-sonar data (20-km swath) to map areas of high backscatter that we infer to represent thinly sedimented crust (≤10m).

Conversion of picked reflection times to sediment thickness in meters was made based on compressional-wave velocity data derived from the DTAGS experiment. We constructed a best-fit polynomial and integrated over travel time to derive the relationship

$$H = 1520\ t\ (1.038\ t^{1/2} + 1),$$

where H = sediment thickness in meters, and t = one-way travel time from seafloor to basement in seconds. Derived sediment thicknesses were contoured at 50-m intervals on six separate maps (Figure 6) at an original scale of 1:200,000.

Regionally, there is no detectable blanket of continuous pelagic sediment cover. Structural highs, such as abyssal hills, and fault scarps have sediments <10 m thick, and bare-rock outcrops appear to be common even on crust as old as 29 Ma. High backscatter in HMR1 data and 3.5-kHz profiles show that crust on the inner rift-valley floor (from zero-age crust of the neovolcanic zone to the first major valley-bounding faults at ~0.5 - 0.7 Ma) has no detectable sediment cover, i.e., total sediment accumulation does not exceed a few meters. On the upper rift-valley walls and on the ridge flank, nearly all structural lows have sediment ponds of varying thicknesses (Figure 6).

The thickest sediments occur in ponds within ridge-parallel valleys between abyssal hills and particularly within the valleys of the non-transform discontinuities in the ridge flank. The ponded sediments in the ridge-parallel valleys are (exceptionally) up to 600 m thick, but thicknesses more typically range from ~50 m to 350 m. These pond surfaces deepen gradually toward the discontinuities, and therefore the valley floors serve as pathways for sediment transport towards segment ends. The non-transform discontinuities contain the thickest sediments, typically up to 500 m and locally up to 800 m.

Total average sediment accumulation versus age was derived in 1-m.y. age bins from the rift axis out to 29 Ma crust (Figure 7). A relatively steady increase in total

sediment accumulation is observed with increasing crustal age up to ~17 Ma crust. Farther off-axis, average sediment accumulation slowly decreases to 20 - 25 m at the western edge of the survey (~29 Ma crust). The observation that >17 Ma seafloor has less sediment is best explained by a depression of the calcite compensation depth to a depth below the crest of the Mid-Atlantic Ridge beginning about 17 Ma.

Brittle Extension of Slow-Spreading Ocean Crust

We developed a new, semi-automated fault-detection and measurement technique to analyze multibeam bathymetry and to quantitatively study the brittle strain taken up by faults (Jaroslow, 1997). We also interpreted backscatter images acquired with the HMR1 sidescan-sonar system to assist in fault identification. The fault-detection technique is well suited to quantitatively characterize regional fault geometry, and it allowed us to compare spatial and temporal variability of faulting in three ridge segments that reach ~300 km off-axis to 20 Ma crust on the ridge flank.

Analyses of the resulting fault data from the western flank of the Mid-Atlantic Ridge provide very significant new constraints on the role of faulting in the formation of topography at slow-spreading ridges. The following summarizes our principal results.

1. Creation of rift-valley and abyssal-hill topography is controlled by faulting on both inward-facing and outward-facing normal faults (Figure 8). Uplift of crust from the rift-valley floor to the crest of the rift mountains is accommodated by extension on normal faults that dip toward the ridge axis, with slip being concentrated on faults near the base of the rift-valley walls (Figure 9). Reduction of rift-valley relief at the crest of the rift mountains is accomplished by outward-facing faults that are active in the upper rift-valley walls. Outward-facing faults account for 40% of the faults observed on the ridge flank. The generation of pairs of inward- and outward-facing faults creates horst and graben terrain that forms most abyssal hills (Figure 2). The dip directions of faults within the walls of the rift valley appear not to be controlled by thermal gradients near the ridge axis, but rather may result from the development of a decoupling horizon near the base of the crust, caused by near-axis formation of serpentinites (Figure 9). This decoupling zone, together with rotation of the axis of maximum principal compressive stress associated with lithosphere necking, favors the formation of outward-facing faults in the upper rift-valley walls. There is no significant faulting beyond the crest of the rift mountains on >3-4 Ma crust.

2. Fault populations show strong differences in geometry, density and strain with intrasegment tectonic setting. Observations on inside-corner crust are consistent with faulting of relatively thick, cold lithosphere with limited magmatic extension; strains are

large and fault spacings tend to be greater than those at segment centers. At segment centers, faults are longer, more linear, more closely spaced, and have smaller offsets and lower strains; this pattern suggests a thinner brittle lid and more magmatic extension. Comparison of brittle strain between individual ridge segments suggests that strain near segment ends is enhanced as the magnitude of offset increases at the non-transform discontinuities between segments.

3. Short-term (~3 m.y.) temporal variations in brittle strain are observed off-axis on the ridge flank, and they most likely reflect changes in magmatic versus relatively amagmatic extension at the ridge axis. Regionally, high fault density and high fault strain correlate with increased residual mantle Bouguer anomaly (i.e., thin crust) attributable to relatively amagmatic extension. Similarly, low fault densities and low strains correlate with reduced residual mantle Bouguer anomaly (thicker crust) attributable to more magmatic extension.

Quantitative Analysis of Abyssal Hills

The multibeam bathymetry acquired during Ewing Cruise 9208 presented a first opportunity to do an extensive regional analysis of morphology of the abyssal hills created at a slow-spreading ridge, and we investigated the relationship between abyssal hills and the properties of the ridge axis at which they were formed (Goff et al., 1995). We applied the Goff-Jordan method to estimate two-dimensional statistical properties of abyssal-hill morphology in three spreading segments, deriving root-mean-square (rms) height, characteristic width, and plan view aspect ratio. The study was done in two parts: 1) analysis of near-axis (<7 Ma) abyssal hills for each of the three segments, and 2) analysis of temporal variations (2-29 m.y. off-axis) in abyssal-hill morphology along the run of the southernmost segment. The results of the analysis were compared with the residual mantle Bouguer gravity data and with preliminary determination of fault characteristics derived from HMR1 sidescan-sonar data.

We found that abyssal-hill morphology is strongly influenced by the inside-corner / outside-corner geometry of the spreading segments. Abyssal hills forming at inside corners have larger rms height and characteristic width and smaller plan-view aspect ratio than those originating at outside corners. The residual mantle Bouguer gravity anomaly is positively correlated with intersegment and along-flow-line variations in rms height and characteristic width, and it is negatively correlated with the plan-view aspect ratio. From this result, we infer that lower-relief, narrower, and more elongated abyssal hills are produced when the crust being generated is thicker. Intersegment variations in near-axis

rms height negatively correlate with average fault density as determined from analysis of HMR1 sidescan-sonar imagery.

Fast-Propagating Rifts in Slow-Spreading Crust

Within the spreading segments identified in the Acoustic Reverberation Corridor, we found a number of highly oblique structural perturbations that cut across the full segment length between bounding non-transform discontinuities (Tucholke et al., 1995; Kleinrock et al., 1996, submitted). The best developed of these features are a pair of structures which appear in ca. 11 Ma and 15 Ma crust within a robust, long-lived spreading segment at 26°N (bold dashed lines, Figure 3). Through time, the structures cut progressively from north to south across the segment, but they did not significantly alter its overall length or integrity. Each structure is characterized by a pronounced morphological depression, by truncation of normal abyssal hills, and by a right-lateral offset of magnetic anomalies. We interpret these structures to have been formed by rapid southward propagation of small (5-7 km), right-lateral offsets of the rift axis. They developed in crust with a spreading half-rate of 14-15 km/m.y., and they propagated at a rate of 25-30 km/m.y.

For such southward propagation and right-lateral anomaly offset, each observed rift trace on the western flank of the Mid-Atlantic Ridge represents an inner pseudofault (IPF) zone, a region of sheared lithosphere transferred from the African to the North American plate. The IPFs have distinct gravity signatures; they mark a relatively rapid transition from a reduced residual mantle Bouguer anomaly in older crust to an elevated anomaly in younger crust, thus suggesting a change from thicker to thinner crust. We interpret the propagation of each of these small discontinuities to have been triggered by the onset of an episode of relatively amagmatic extension.

The other propagators within the survey region have the same essential features, including IPF tectonic setting, but they are not as robustly developed. All observed propagators migrated southward. However, it is difficult to distinguish subtle magnetic-anomaly perturbations at outer pseudofaults of possible northward-propagating rifts in this slow-spreading environment, so this observation may be an artifact rather than an indicator of preferred direction of propagation.

Seamount Volcanism: Origin and Evolution of Ridge-Flank Seamounts

We identified 86 axial seamounts and 1290 off-axis seamounts (near-circular volcanoes) that are ≥ 60 m high in the Acoustic Reverberation Corridor out to ~29 Ma crust (Figure 10; Jaroslow et al., 1994, 1995, 1996; Jaroslow, 1997). We developed a new, on-screen interactive computer program to record latitude, longitude, and minimum depth

of each seamount top, as well as latitude, longitude, and water depth of the endpoints of the minimum and maximum plan-view shape axes. From these data we derived the following shape parameters: minimum basal diameter, D_{min}; maximum basal diameter, D_{max}; average basal water depth, D_b, taken as the average of the four basal depths recorded; seamount height, h, the difference between D_b and summit depth; height-to-diameter ratio, $\xi_d = h/D_b$; and ϕ_{max}, the strike of D_{max}.

We also studied the seamounts in HMR1 long-range sidescan-sonar data to determine their geological relations and age with respect to the surrounding seafloor. Seamount population and shape parameters were analyzed to determine the temporal evolution of seamounts and also to evaluate the nature and causes of any along-isochron variation within individual spreading segments. The major conclusions of our study are summarized as follows:

1. Analysis of sidescan-sonar images and multibeam bathymetric data shows no evidence that seamounts are constructed off-axis. Seamounts appear to originate primarily on the inner rift-valley floor of the Mid-Atlantic Ridge, so the seamounts observed on the ridge flank have survived faulting and transport out of the rift valley.

2. The abundance of off-axis seamounts demonstrates that large sections of ocean crust are carried intact from the rift-valley floor through the rift-valley walls and onto the ridge flank (>4 Ma crust). However, there are significant changes in seamount population density, size distribution, and shape between ridge axis and ridge flank, and these are caused by faulting between ~0.6 and 3 - 4 m.y. off-axis in the rift-valley walls (Figure 11). During initial transport of seamounts from the rift valley (0.6 - 2 m.y.), few seamounts are destroyed by (inward-facing) faults, but seamount height is significantly decreased. In the upper portions of the rift-valley wall, on crust 2 - 4 Ma, additional faults (outward-facing) destroy and degrade a significant number of seamounts. These results are consistent with evidence, noted earlier, that outward-facing faults appear in the upper portions of the rift-valley walls.

3. Beyond the crest of the rift mountains (>4 Ma), faulting is no longer active, and changes in the off-axis seamount population reflect long-period crustal aging processes and temporal changes in seamount production that occurred at the ridge axis. A steady decline in characteristic height of the seamount population with crustal age is observed beyond about 4 m.y. off-axis and is attributed to the cumulative effects of mass-wasting. A marked increase in seamount population density on ~20 - 24 Ma crust may have been caused by an increase in axial seamount production at that time, or it may reflect a decrease in seamount destruction that is related to reduced density of faults.

4. Population density of off-axis seamounts has a positive correlation with crustal thickness (as inferred from residual mantle Bouguer gravity data; Figure 5), suggesting that increased seamount production accompanies increased magma input to the rift valley. However, intra-segment variations in seamount population characteristics do not appear to correlate with inside-corner, segment-center, or outside-corner tectonic setting, or to associated differences in residual gravity anomaly. It is unclear whether this effect is real or whether it is an artifact of the way the tectonic settings were defined in our study (i.e., as percentages of segment length, rather than as detailed, but subjectively interpreted, geological boundaries).

5. There are no variations in observed seamount population density with along-isochron position in individual ridge segments. There are two possible explanations: a) Along-axis production of seamounts is actually uniform, in which case melt delivery in the shallow crust must also be relatively uniform along-axis, irrespective of how it is supplied to the base of the crust by deep-seated magmatic processes. b) Seamount production varies along-axis, but along-axis variations in the style of volcanism prevent its topographic identification. In particular, complete or partial burial of segment-center seamounts by subsequent volcanic flows might reduce seamount population density and characteristic heights to values similar to those at segment ends.

Fine-Scale, Near-Bottom Surveys on the Mid-Atlantic Ridge Flank

We conducted detailed near-bottom, high-resolution surveys of the seafloor on Knorr Cruise 138-14 in 1993 (Kleinrock et al., 1993; Shaw et al., 1993b; Tucholke et al., 1993). We used the ROV Jason and the DSL-120 deep-towed sonar system at four locations (Sites A, B, C, D) on the western flank of the Mid-Atlantic Ridge. All sites were adjacent to a non-transform discontinuity that segments the ridge flank. Sites C and D were on inside-corner crust, Site A was on outside-corner crust, and Site B was on segment-center to outside-corner crust. Navigation accurate to a few meters was provided by undithered surface-ship GPS and by bottom-transponder networks. We collected sidescan backscatter amplitude and phase-difference bathymetry (120 kHz, 200 kHz); forward-scan sonar (300 kHz); precision pencil-beam bathymetry; magnetics; video, film, and electronic still photography; and seafloor rock samples. Auxiliary seafloor samples were recovered by dredging during the acoustics cruise that immediately followed our work (Knorr Cruise 138-15).

The near-bottom surveys showed three primary types of seafloor features: 1) relatively low-slope to level, sediment-covered ponds and terraces, 2) moderate-slope (20°-40°) talus ramps that are 60-90% sediment covered, and 3) steep-slope (40°-90°, locally overhanging)

scarps that vary in height from a few tens of meters to more than 200 meters. Terraces typically are bounded upslope by the talus ramps, and the talus ramps lie at the bases of scarps. Most scarps appear to be formed either by faulting or as local headwalls of slides. The scarps typically exhibit truncated pillow-basalt structures or show slab-like faces that may be zones of fault gouge.

At Site B (~24 Ma crust), sidescan-sonar data show linear zones of faults that parallel seafloor isochrons, although individual fault scarps exhibit great variability in structure and orientation. The basaltic crust is thickly covered by iron-manganese coatings several centimeters thick, and only rare fresh faces are exposed by mass wasting.

Sonar data at Site C (~17 Ma crust) also show some linear fault zones, but many roughly equidimensional basement features crop out through the sediment cover. The inside-corner tectonic setting of this crust suggests that the features may be formed by serpentinite diapirism and that the basement may be dominated by lower-crustal and upper-mantle rocks with little basaltic overburden.

Sidescan-sonar images of outside-corner crust at Site A (~11 Ma crust) show well lineated fault zones like those at Site B. Fine-scale ROV Jason study at Site A concentrated on a 180-m-high seamount and shows exposed basalts that are shattered and faulted into locally steep scarps with basal talus ramps. Manganese coating on the basalts is strongly reduced in comparison to older crust.

Site D was on thinly sedimented, ~4 Ma crust. Irregularly oriented, near-vertical fault scarps up to 200 m high occur in a basaltic carapace on the inside corner. A survey line run onto adjacent outside-corner crust shows smaller-throw faults and numerous small volcanic cones. The fine-scale survey data greatly extend, and generally confirm, interpretations of inside- and outside-corner crustal structure made from larger-scale multibeam bathymetry and long-range sidescan-sonar data.

Denudation and Mass-Wasting of Ocean Crust

Our near-bottom surveys provided the first detailed data on long-term denudation processes that modify basement topography away from the Mid-Atlantic Ridge axis (Tucholke et al., 1994; in press, a). Near-axis, the igneous crust is exposed in fault scarps that easily degrade, but our off-axis data show that the scarps can be subjected to significant denudation for periods up to 10-20 m.y. or more. This work provided unique new insights into the processes and products of such long-term denudation.

The principal mechanism of denudation appears to be mass wasting (gravitational failure), including slumps and slides at scales up to 1 km or more. Debris flows and turbidity currents probably form by disaggregation of small failed blocks, and they may

contribute significantly to erosion of canyons and gullies through abrasion. Scarp failure is thought to be facilitated largely by intracrustal weathering in preexisting zones of weakness such as faults, fissures, and flow contacts. Seismic shock probably is important in triggering failure within the seismically active rift valley (≤2 Ma), but it becomes less effective with distance onto the relatively aseismic ridge flank.

Initial denudation forms cross-scarp chutes and gullies. With time, these develop into canyons that cut progressively deeper into scarps and are joined by scarp-parallel gullies to create trellis drainage patterns (Figures 12 and 13). This process continues out to crust at least 24 m.y. old, although the rate of denudation probably diminishes with time as slopes decrease. In mature trellis drainage, resistant ridges commonly are reduced to sharp-edged, arete-like form by lateral denudation in the walls of adjacent canyons and gullies. Development of trellis patterns appears to result from excision of rock in structurally weak zones, i.e., along faults and fractures that formed in a roughly rectilinear pattern near the ridge axis and that were subjected to intracrustal weathering. The long temporal record of scarp failure suggests that exposed scarps are not significantly stabilized off-axis by secondary mineralization and sealing in the weak zones. Canyon-cutting into exposed scarps proceeds at average rates of 10-20 m/m.y.; the steepest dips along original scarp faces are reduced from >50° on 4 Ma crust to 35°-40° on 24 Ma crust, and scarp widths markedly increase.

These changes in morphology and slope are important to consider in studies of acoustic backscatter from the ocean crust. They also are important to tectonic interpretations. Brittle strain taken up by faults, if computed from apparent fault dips of degraded scarps rather than from careful reconstruction of true dips, will be strongly overestimated, and strain derived in this way could appear fallaciously to increase with age.

Multi-Scale Spectral Analysis of Seafloor Bathymetry

We conducted a multi-scale spectral analysis of Hydroweep multibeam and Mesotech scanning pencil-beam bathymetric data from the Acoustic Reverberation Corridor on the flank of the Mid-Atlantic Ridge (Goff and Tucholke, in press). These data were augmented by visual data which enabled us to identify bathymetric profiles that are over unsedimented or thinly sedimented crust. Our analysis thus focused primarily on statistical characterization of basement morphology. We concentrated on two sites: Site B on ~24 Ma crust in a segment-center to outside-corner tectonic setting, and Site D on ~4 Ma crust in an inside-corner setting.

At Site B we found that an anisotropic, band-limited fractal model (i.e., the "von Kármán" model of abyssal hill morphology) is not sufficient to describe the full range of

scales observed. Our observations differ from the model in two ways: 1) strike and cross-strike (dip) spectral properties converge for wavelengths smaller than ~300m, and 2) in both strike and dip directions the fractal dimension changes at ~10 m wavelength, from ~1.27 at larger scales to ~1.0 at smaller scales. The convergence of strike and dip spectral properties appears to be associated with destruction of ridge-parallel fault scarps by mass wasting, which develops canyon-like incisions that cross scarps at high angles (Figure 12). The change in fractal dimension at ~10 m scale appears to be related to a minimum spacing of significant slope breaks associated with scarps which are created by faulting and mass wasting.

At Site D, although there is no significant abyssal-hill anisotropy, the spectral properties at all scales are consistent with the von Kármán model. The fractal dimension at this site (~1.15) is less than at Site B. This difference may reflect different morphology related to crustal formation in an inside- versus outside-corner tectonic setting or, more likely, it reflects differences in the degree of mass wasting. The smoothing of seafloor morphology by sediments is evident in Hydrosweep periodograms where, relative to basement roughness, spectral power decreases progressively with decreasing wavelength.

Numerical Analysis of Acoustic Reverberation Data in the Acoustic Reverberation Corridor

Acoustic seafloor-scattering data contain information about fine-scale seafloor morphology. The fine-scale, near-bottom data on seafloor structure and bathymetry that we acquired during Knorr Cruise 138-14 were used by ARSRP acousticians to model acoustic scatter from the seafloor within the Acoustic Reverberation Corridor.

Our work with ARSRP acousticians (Robertsson et al., 1996, submitted) integrated acoustics and geology studies of the seafloor. In this research, a 2-D hybrid wave-propagation simulation technique was employed to simulate acoustic scattering from the seafloor on the Mid-Atlantic Ridge flank, using a stochastic representation of fine-scale bathymetry observed in near-bottom surveys. Overall, the arrival in time, the level, and the shape of the events in the simulated data match actual acoustic data well. The results indicate that noise significantly reduces the dynamic range and quality of the acoustic data.

Other important results are: 1) The seafloor must be deterministically known to a very fine scale (on the order of 10 m) to allow accurate prediction of the principal events in the reverberated signal. 2) To reduce 3-D effects, the modeled beam must be oriented perpendicular to the lineation of the seafloor. Strong out-of-beam events may also appear in the beam-formed data. 3) To some extent, a finite cross-range resolution reduces 3-D

effects within the "foot-print" of the beam in the acoustic data. However, too large a foot-print may violate the 2-D approximation.

Summary Geological Model of Spreading Segments in Slow-Spreading Crust

Our surveys and studies in the ONR Atlantic Natural Laboratory and the Acoustic Reverberation Corridor provided an exceptional and unprecedented opportunity to develop new insights into the morphology, structure, origin, and evolution of slow-spreading ocean crust. From these studies, we were able to develop a general geological model of the structure of ridge segments in slow-spreading crust (Tucholke and Lin, 1994), summarized below.

Transform and non-transform ridge-axis discontinuities create a fundamental segmentation of the lithosphere along slow-spreading mid-ocean ridges, and they commonly are associated with exposure of subvolcanic crust and upper mantle. We analyzed available morphological, gravity, and rock sample data from the Acoustic Reverberation Corridor and throughout the Atlantic Ocean to determine whether consistent structural patterns occur at these discontinuites and to constrain the processes that control the patterns.

The results show that along their older, inside-corner sides, both transform and non-transform discontinuities are characterized by thinned crust and/or mantle exposures as well as by irregular fault patterns and a paucity of volcanic features. Crust on young, outside-corner sides of discontinuities has more normal thickness, regular fault patterns, and common volcanic forms. These patterns are consistent with tectonic thinning of crust at inside corners by low-angle normal (detachment) faults. Volcanic upper crust accretes in the hanging wall of the detachment, is stripped from the inside-corner footwall, and is carried to the outside corner. Gravity and morphological data suggest that detachment faulting is a relatively continuous process in crust spreading at <25-30 mm/yr, that it may be intermittent at intermediate rates of 25-40 mm/yr, and that it is unlikely to occur at faster rates. Detachment surfaces are dissected by later, high-angle faults formed during crustal uplift into the rift mountains; these faults can cut through the entire crust and may be the kinds of faults imaged by seismic reflection profiling over older crust in the North Atlantic.

Off-axis variations in gravity anomalies indicate that slow-spreading crust experiences cyclic magmatic/amagmatic extension and that a typical cycle is about 2-3 m.y. long. During magmatic phases the footwall of the detachment fault probably exposes lower-crustal gabbros, although these rocks locally may have an unconformable volcanic

carapace. During amagmatic extension the detachment may dip steeply through the crust, providing a mechanism whereby upper mantle ultramafic rocks can be exhumed very rapidly, perhaps in as little as 0.5 m.y. Together, detachment faulting and cyclic magmatic/amagmatic extension create strongly heterogeneous lithosphere both along and across isochrons in slow-spreading ocean crust.

SCIENTIFIC IMPACT

The geological and geophysical surveys conducted in this program have provided 1) an off-axis record of Mid-Atlantic Ridge crustal structure and evolution that is much longer and more detailed than any other in the ocean basins, and 2) a complete, multi-scale spectrum of geological and geophysical observations of the ocean crust. As a result, we have gained fundamental new insights into the structure and morphology of ocean crust and its sedimentary load, as well as a greatly improved understanding of processes that control the origin and variability of these features. These data provide unique and essential information that is necessary to model and understand acoustic interaction with the seabed over large areas of the deep ocean basins.

BIBLIOGRAPHY OF RESEARCH SUPPORTED BY THIS GRANT

Research Papers in Scientific Journals

Goff, J.A., B.E. Tucholke, J. Lin, G.E. Jaroslow, and M.C. Kleinrock, Quantitative analysis of abyssal hills in the Atlantic Ocean: A correlation between crustal thickness and extensional faulting, J. Geophys. Res., 100, 22,509-22,522, 1995.

Goff, J. A., and B. E. Tucholke, Multi-scaled spectral analysis of seafloor bathymetry on the flanks of the Mid-Atlantic Ridge, J. Geophys. Res. (in press).

Jaroslow, G.E., and B.E. Tucholke, Mesozoic-Cenozoic sedimentation in the Kane Fracture Zone, Western North Atlantic, and uplift history of the Bermuda Rise, Geological Society of America Bulletin, 106, 319-337, 1994.

Kleinrock, M.C., B.E. Tucholke, J. Lin, and M.A. Tivey, Fast rift propagation at a slow-spreading ridge: Progressive tearing of an entire spreading segment, Geology (submitted).

Robertsson, J.O.A., K. Holliger, A. Levander, J.A. Goff, H.F. Webb and B.E. Tucholke, A numerical analysis of ocean acoustic reverberation data from the proximity of the Mid-Atlantic Ridge, J. Acoust. Soc. America (submitted).

Tivey, M.A., and B.E. Tucholke, Magnetization of oceanic crust from 0 to 29 Ma formed at the Mid-Atlantic Ridge 25°30' to 27°10'N, J. Geophys. Res. (submitted).

Tucholke, B.E., Massive submarine rockslide on the rift valley wall of the Mid-Atlantic Ridge, Geology, 20, 129-132, 1992.

Tucholke, B.E., K.C. Macdonald, and P.J. Fox, ONR seafloor natural laboratories on slow- and fast-spreading mid-ocean ridges, EOS Trans. Am. Geophys. Union, 72, 268-270, 1991.

Tucholke, B.E., and J. Lin, A geological model for the structure of ridge segments in slow-spreading ocean crust, J. Geophys. Res., 99, 11,937-11,958, 1994.

Tucholke, B.E., W.K. Stewart, and M.C. Kleinrock, Long-term denudation of ocean crust in the central North Atlantic Ocean, Geology (in press, a).

Tucholke, B.E., J. Lin, M.C. Kleinrock, M. Tivey, T.B. Reed, J. Goff, and J. Jaroslow, Segmentation and crustal structure of the western Mid-Atlantic Ridge flank, 25°30' - 27°10' and 0 - 29 m.y., J. Geophys. Res. (in press, b).

Ph.D. Theses

Jaroslow, G.E., The Geological Record of Oceanic Crustal Accretion and Tectonism at Slow-Spreading Ridges, Ph.D. Thesis, Massachusetts Institute of Technology - Woods Hole Oceanographic Institution Joint Program in Oceanography, 210 pp., 1997.

Miscellaneous Publications

Tucholke, B.E., K.C. Macdonald, and P.J. Fox, ONR Seafloor natural laboratories on the Mid-Atlantic Ridge and East Pacific Rise, Ridge Events, 2(1), 15-18, 1991.

Tucholke, B.E., Geologists investigate spatial variability and temporal cycles of Atlantic Ocean crust formation, Woods Hole Oceanographic Institution Annual Report 1992, p. 13, 1993.

Kleinrock, M.C., B.E. Tucholke, and J. Lin, Ridge segmentation, migrating offsets, and crustal structure on the western flank of the Mid-Atlantic Ridge from 25°25'N to 27°10'N to 30 Ma., Ridge Events, 3(2), 5-7, 1992.

Tucholke, B.E., Geologists map the fine-scale structure of Atlantic Ocean crust, Woods Hole Oceanographic Institution Annual Report 1993, p. 13, 1993.

Abstracts of Oral Presentations

Goff, J. A., M.C. Kleinrock, J. Lin, and B. Tucholke, Quantitative analysis of abyssal hill morphology within three segments: The west flank of the MAR 25°25'N-27°10'N and 0-30 Ma., EOS Trans. Am. Geophys. Union, v. 73, no. 43, p. 538, 1992.

Jaroslow, G.E., D.K. Smith, and B.E. Tucholke, The off-axis record of volcanism in the western North Atlantic Ocean, EOS Trans. Am. Geophys. Union, v. 75, no. 44 (Fall Meeting Supplement), p. 660, 1994.

Jaroslow, G.E., D.K. Smith, and B.E. Tucholke, Production and evolution of seamounts in the ONR Natural Laboratory, North Atlantic Ocean, EOS Trans. Am. Geophys. Union, v. 76, no. 46 (Fall Meeting Supplement), p. F553-F554, 1995.

Jaroslow, G.E., D.K. Smith, and B.E. Tucholke, Seamount production and evolution in the western North Atlantic Ocean, 25°30' - 27°10'N: FARA-InterRidge Mid-Atlantic Ridge Symposium, 19-22 June 1996, Reykjavik, Iceland, Journal of Conference Abstracts, v. 1, p. 802, 1996.

Jung, W., P. Vogt, J. McCune, and B.E. Tucholke, Variability of the acoustic backscatter strengths in a northern Mid-Atlantic Ridge west flank, EOS Trans. Am. Geophys. Union, v. 74, no. 43, p. 342, 1993.

Kleinrock, M.C., B.E. Tucholke, J. Lin and M.A. Tivey, The trace of non-transform offsets and the evolution of Mid-Atlantic Ridge spreading segments between 25°25'N and 27°10'N over the past 30 m.y., EOS Trans. Am. Geophys. Union, v. 73, no. 43, p. 538, 1992a.

Kleinrock, M.C., B.E. Tucholke, and J. Lin, HAWAII MR1 sidescan sonar survey of the Mid-Atlantic Ridge rift valley from 25°25'N to 27°N, EOS Trans. Am. Geophys. Union, v. 73, no. 43, p. 567, 1992b.

Kleinrock, M.C., and B.E. Tucholke, Evidence from towed and remotely operated vehicles for variations in the structure of the traces of nontransform offsets at the Mid-Atlantic Ridge, EOS Trans. Am. Geophys. Union, v. 74, no. 43, p. 574, 1993.

Kleinrock, M.C., B.E. Tucholke, and J. Lin, Geometry and structure of inside corners and pseudofaults at a slow-spreading ridge, EOS Trans. Am. Geophys. Union, v. 77, no. 46 (Fall Meeting Supplement), p. F723, 1996.

Lin, J., B.E. Tucholke, M.C. Kleinrock, and J.A. Goff, Variations in crustal faulting and magmatic accretion along the Mid-Atlantic Ridge and off-axis: results from the western flank of the MAR at 25-27 deg N, EOS Trans. Am. Geophys. Union, v. 73, no. 43, p. 538, 1992.

Lin, J., B.E. Tucholke and M.C. Kleinrock, Off-axis "boudin-shaped" gravity lows on the western flank of the Mid-Atlantic Ridge at 25°25'N-27°10'N: Evidence for long-term pulses in magmatic accretion in spreading segments, EOS Trans. Am. Geophys. Union, v. 74, no. 16, p. 380, 1993a.

Lin, J., B.E. Tucholke, and M. Kleinrock, Evidence from gravity and morphology for long-term variability in magmatic vs. tectonic extension at the Mid-Atlantic Ridge, EOS Trans. Am. Geophys. Union, v. 74, no. 16, p. 303, 1993b.

Lin, J., B.E. Tucholke, M.C. Kleinrock, and J. Escartin, Contrasting inside- vs. outside-corner crustal structure on flanks of a slow-spreading ridge, EOS Trans. Am. Geophys. Union, v. 76, no. 46 (Fall Meeting Supplement), p. F554, 1995.

Lin, J., B.E. Tucholke, M.C. Kleinrock, and J. Escartin, Along- and across-isochron gravity and bathymetric anomalies on the Mid-Atlantic Ridge: Implications for tectonics of slow-spreading crust, EOS Trans. Am. Geophys. Union, v. 77, no. 46 (Fall Meeting Supplement), p. F724, 1996.

Reed, T.B, IV, D. Smith, B.E. Tucholke, Multi-source, multi-scale imagery of the MAR, 25° - 27° North, EOS Trans. Am. Geophys. Union, v. 73, no. 43, p. 552, 1992.

Reed, T.B., D.K. Smith, and B.E. Tucholke, Multi-source, multi-scale imagery of the MAR, 25-27 deg. North, International Conference on Acoustic Classification and Mapping of the Seabed, 14-16 April 1993, Univ. of Bath, England, 1993.

Shaw P.R., B.E. Tucholke, and J. Lin, Large-scale tectonic fabric of the northern Mid-Atlantic Ridge flank, EOS Trans. Am. Geophys. Union, v. 74, no. 16, p. 306, 1993a.

Shaw, P.R., M.C. Kleinrock, and B.E. Tucholke, Multiscale analysis of the tectonic fabric of the northern Mid-Atlantic Ridge flank, EOS Trans. Am. Geophys. Union, v. 74, no. 43, p. 574, 1993b.

Shaw, P.R., M.A. Tivey, B.E. Tucholke, M.C. Kleinrock, and J. Lin, Past plate motions recorded in abyssal hill lineations and magnetic lineations on the western flank of the MAR, 26N, EOS Trans. Am. Geophys. Union, v. 75, no. 16 (Spring Meeting Supplement), p. 330, 1994.

Tucholke, B. E., and J. Lin, Asymmetric crustal structure at ridge-axis offsets, Mid-Atlantic Ridge, EOS Trans. Am. Geophys. Union, v. 72, p. 467, 1991.

Tucholke, B.E., J. Lin, and T.B. Reed IV, Patterns of seafloor faulting and volcanic morphology observed along- and across-axis on the Mid-Atlantic Ridge, 24°-27°N, EOS Trans. Am. Geophys. Union, v. 72, p. 260, 1991a.

Tucholke, B.E., T.B. Reed IV, and J. Lin, Bottom roughness of the Mid-Atlantic Ridge flank observed in SeaMARC II sidescan sonar and SeaBeam multibeam bathymetry, Journal Acoustical Soc. America , v. 90, p. 2236, 1991b.

Tucholke, B.E., and J. Lin, Detachment faulting and its relation to geologic structure at first-and second-order offsets of slow-spreading ridges, EOS Trans. Am. Geophys. Union, v. 73, p. 286, 1992.

Tucholke, B.E., J. Lin, and M.C. Kleinrock, Crustal structure of spreading segments on the western flank of the Mid-Atlantic Ridge at 25°25'N to 27°10'N, EOS Trans. Am. Geophys. Union, v. 73, no. 43, p. 537, 1992a.

Tucholke, B.E., M.C. Kleinrock, W.K. Stewart, J. Lin, J. Goff, G. Jaroslow, B. Brooks, P. Lemmond, J. Howland, M. Marra, T. Reed, M. Edwards, J.R. Fricke, U. Herzfeld, Geological and geophysical survey of the Mid-Atlantic Ridge flank at 25°25'N to 27°10'N, EOS Trans. Am. Geophys. Union, v. 73, no. 43, p. 552, 1992b.

Tucholke, B.E., M. Kleinrock, and W.K. Stewart, Fine-scale, near-bottom surveys of ocean crust on the flank of the Mid-Atlantic Ridge, 26 to 27 degrees North, EOS Trans. Am. Geophys. Union, v. 74, no. 43, p. 574, 1993.

Tucholke, B.E., W.K. Stewart, and M.C. Kleinrock, Dissection and degeneration of fault scarps observed by fine-scale survey of slow-spreading ocean crust, EOS Trans. Am. Geophys. Union, v. 75, no. 44 (Fall Meeting Supplement), p. 649, 1994.

Tucholke, B.E., M.C. Kleinrock, M. Tivey, and J. Lin, Fast-propagating rifts in slow-spreading crust, EOS Trans. Am. Geophys. Union, v. 76, no. 46 (Fall Meeting Supplement), p. F554, 1995.

Tucholke, B.E., Structure of mid-ocean ridges, NAGT Symposium, Plate Tectonics, What Students Should Know; Geol. Soc. Am. Abstr. with Programs, v. 28, no. 7, p. A-223, 1996.

Tucholke, B.E., J. Lin, and M.C. Kleinrock, Off-axis structure of spreading segments on the Mid-Atlantic Ridge flank near 26°N, ODP-InterRidge-IAVCEI Workshop, The Oceanic Lithosphere and Scientific Drilling into the 21st Century, 26-28 May 1996, North Falmouth, MA, p.111, 1996a.

Tucholke, B.E., J. Lin, and M. C. Kleinrock, Mullions, megamullions, and metamorphic core complexes on the Mid-Atlantic Ridge, EOS Trans. Am. Geophys. Union, v. 77, no. 46 (Fall Meeting Supplement), p. F724, 1996b.

Abstracts of Presentations at ARSRP Research Symposia

Tucholke, B.E., J. Lin, and T.B. Reed IV, Patterns of seafloor morphology observed along- and across-axis on the Mid-Atlantic Ridge 24°-27° N, Second Annual Acoustic Reverberation Special Research Program Symposium, 20-22 March 1991, Scripps Inst. Ocean., La Jolla, CA, p. 4, 1991.

Tucholke, B.E., Geological and geophysical survey of the Acoustic Reverberation Corridor, Mid-Atlantic Ridge, Second Annual Acoustic Reverberation Special Research Program Symposium, 20-22 March 1991, Scripps Inst. Ocean., La Jolla, CA, p. 5, 1991.

Jaroslow, G., and B. Tucholke, Echo character of the Mid-Atlantic Ridge flank in the region of the Acoustic Reverberation Corridor, Acoustic Reverberation Special Research Program, 1991 Fall Research Symposium, 24-25 September 1991, Woods Hole Ocean. Inst., Woods Hole, MA, p. 15, 1991.

Tucholke, B. E., and J. Lin, Initial model for the geologic structure of Mid-Atlantic Ridge oceanic crust offset by small ridge-axis discontinuities, Acoustic Reverberation Special Research Program, 1991 Fall Research Symposium, 24-25 September 1991, Woods Hole Ocean. Inst., Woods Hole, MA, p. 30, 1991.

Tucholke, B.E., M.C. Kleinrock, and P. Lemmond, Geology and geophysics reconnaissance survey of the Acoustic Reverberation Corridor, Acoustic Reverberation Special Research Program, 1992 Spring Research Symposium, 7-9 April 1992, Scripps Inst. Ocean., La Jolla, CA, p. 33, 1992.

Goff, J.A., M.C. Kleinrock, J. Lin, and B. Tucholke, Quantitative analysis of abyssal hill morphology within three segments: The west flank of the MAR at 25°25'N - 27°10'N and 0-3 Ma, Acoustic Reverberation Special Research Program, 1992 Fall Research Symposium, 18 - 20 November 1992, Woods Hole Ocean. Inst., Woods Hole, MA, p. 14, 1992.

Reed, T.B. IV, D. Smith, and B.E. Tucholke, Multi-source, multi-scale imagery of the MAR, 25°-27° North, Acoustic Reverberation Special Research Program, 1992 Fall Research Symposium, 18 - 20 November 1992, Woods Hole Ocean. Inst., Woods Hole, MA, p. 20, 1992.

Tucholke, B.E., M.C. Kleinrock, J. Lin, and W.K. Stewart, Geological and geophysical survey of the Acoustic Reverberation Corridor on the west flank of the Mid-Atlantic Ridge at 25°25'N to 27°10'N, Acoustic Reverberation Special Research Program, 1992 Fall Research Symposium, 18 - 20 November 1992, Woods Hole Ocean. Inst., Woods Hole, MA, p. 28, 1992.

Tucholke, B.E., Fine-scale, near-bottom geological and geophysical investigations of ocean crust in the ONR ARSRP Acoustic Reverberation Corridor (west flank of the Mid-Atlantic Ridge, 26°-27°N), Acoustic Reverberation Special Research Program, 1992 Fall Research Symposium, 18 - 20 November 1992, Woods Hole Ocean. Inst., Woods Hole, MA, p. 29, 1992.

Tucholke, B.E., M.C. Kleinrock, and W.K. Stewart, Geological and geophysical characteristics of the Acoustic Reverberation Corridor, and their relevance to the conduct of G&G fine-scale surveys, Acoustic Reverberation Special Research Program, 1993 Spring Research Symposium, 23-25 March 1993, Scripps Inst. Ocean., La Jolla, CA, p. 11-14 (extended abstract), 1993.

Caruthers, J.W., and B.E. Tucholke, Geology and geophysics at ARSRP Sites A and C, Acoustic Reverberation Special Research Program, 1993 Spring Research Symposium, 23-25 March 1993, Scripps Inst. Ocean., La Jolla, CA, p. 23, 1993.

Tucholke, B.E., M.C. Kleinrock, and W.K. Stewart, Fine-scale geological and geophysical surveys at Sites B', C', A and D in the Acoustic Reverberation Corridor, Acoustic Reverberation Special Research Program, 1993 Fall Research Symposium, 1-3 December 1993, Scripps Inst. Ocean., La Jolla, CA, p. 16-22 (extended abstract).

Tucholke, B.E., W.K. Stewart, and M.C. Kleinrock, Irregularity of fault scarps in the Acoustic Reverberation Corridor caused by slope failure and mass wasting, Acoustic Reverberation Special Research Program, 1995 Research Symposium, 19-21 July 1995, Woods Hole Ocean. Inst., Woods Hole, MA, 1995.

Jaroslow, G.E., and B.E. Tucholke, Detailed mapping of sediment distribution in the Acoustic Reverberation Corridor, Acoustic Reverberation Special Research Program, 1995 Research Symposium, 19-21 July 1995, Woods Hole Ocean. Inst., Woods Hole, MA, 1995.

FIGURE CAPTIONS

Figure 1 - Location of the ARSRP Acoustic Reverberation Corridor over 0-29 Ma crust on the west flank of the Mid-Atlantic Ridge. The Mid-Atlantic Ridge axis (double line) and off-axis traces of transform faults (labeled) and non-transform discontinuities (light lines) are interpreted from the marine gravity field derived from satellite altimetry. Other detailed surveys along the Mid-Atlantic Ridge extend ~10 m.y. off-axis (ATLANTIS, SARA, and SEADMA).

Figure 2 - Bathymetry of the Acoustic Reverberation Corridor mapped with the Hydrosweep multibeam system during Ewing Cruise 9208. Contour interval is 100 m. Along the Mid-Atlantic Ridge axis, Hydrosweep bathymetry is merged with SeaBeam bathymetry of preexisting surveys.

Figure 3 - Magnetic anomalies and tectonic interpretation of ridge-flank segments (identified by letters) in the Acoustic Reverberation Corridor. Magnetic anomalies are numbered, and crustal ages (Ma) are shown along the top of the figure in parentheses; fine lines locate positive anomalies and heavier lines locate negative (r) anomalies. Non-transform discontinuities, where identifiable in sea-floor morphology, are shown as black heavy lines at right-stepping offsets, as open lines at left-stepping offsets, and as dashed lines where weakly developed. The bold dashed lines in Segment E locate traces of two fast-propagating rifts. Note the major ~9° counterclockwise change in orientation of magnetic anomalies following ~24 Ma (bold lines). Short dashes outline the limit of multibeam bathymetric coverage in Figure 2.

Figure 4 - Plan-view comparison of a submarine megamullion at the inside-corner edge of segment G (left) with "turtleback" metamorphic core complexes exposed in the Chemehuevi and Whipple mountains in southeastern California (right), all at the same scale. a) Bathymetry of the submarine megamullion; contours at 100-m intervals. Solid circle locates dredged serpentinite. b) HMR1 sidescan-sonar image (southward insonification) of the same feature. c) Highly simplified geological map of the subaerial metamorphic core complexes, adapted from the published literature. Both the submarine and subaerial features are thought to have originated by detachment faulting and they have similar scales, roughly equidimensional to elliptical outlines, domed morphology, and internal occurrence of high-angle normal faults orthogonal to the direction of extension.

Figure 5 - Residual mantle Bouguer anomaly (mGal) for the Acoustic Reverberation Corridor. Segment boundaries as in Figure 3. Note the cross-isochron bands of gravity lows at segment centers and gravity highs over inside-corner crust, and the alternating relative highs and lows at ~2-3 m.y intervals within these bands. From the Mid-Atlantic Ridge axis eastward, the residual mantle Bouguer anomaly is taken from Tucholke and Lin (1994).

Figure 6 - Maps of sediment thickness in the Acoustic Reverberation Corridor on the western flank of the Mid-Atlantic Ridge, 0 - 29 Ma crust. Contour interval is 50 m. Black areas have high backscatter in HMR1 sidescan-sonar data and are interpreted to have sediment cover 0 - 10 m thick.

Figure 7 - Bar graph of average sediment thickness versus age over the Mid-Atlantic Ridge flank in the Acoustic Reverberation Corridor. Bin size is 1 m.y.

Figure 8 - Map of all inward-facing (blue) and outward-facing (red) normal faults identified in our fault study (0-20 Ma crust) within the Acoustic Reverberation Corridor. Segment boundaries are marked by gray lines, and the ridge axis is shown by heavy black lines. Thin black lines indicate crustal ages (Ma). The strike of most faults is parallel or subparallel to average plate-boundary orientation, marked by the arrow in the upper left corner. Note that pairs of closely spaced inward- and outward- facing faults are common, and they create elongate horsts that form most abyssal hills.

Figure 9 - Schematic cross-sections of the Mid-Atlantic Ridge from the ridge axis (right) out to ~5.5 Ma crust (no vertical exaggeration) showing our geological model of faulting in the rift valley. Active faults are shown as solid lines and inactive faults are shown as dashed lines. Serpentinites are indicated by the hatched pattern. a) Model for thick crust formed during relatively magmatic extension. Few inward-facing faults reach the base of the crust in the lower rift-valley walls, so seawater rarely penetrates through the crust to facilitate serpentinization of the mantle; outward-facing faults thus form rarely and only in locations where serpentinites create a local, ductile layer at the base of the crust. b) Model for thin crust formed during relatively amagmatic extension. Inward-facing faults commonly extend through the crust and allow seawater penetration to the mantle; thus a ductile upper-mantle serpentinite layer is well developed. Outward-facing faults readily form in the thin, brittle crustal lid as

lithospheric necking rotates the stress field in the rift-valley walls. In both a) and b), slip on faults in crust older than 3-4 Ma is very rare.

Figure 10 - Color bathymetric map of combined SeaBeam and Hydrosweep multibeam bathymetry in the Acoustic Reverberation Corridor, with identified seamounts shown as black dots; dot size is proportional to mean seamount diameter. Segment boundaries and the Mid-Atlantic Ridge axis are indicated by thin white lines.

Figure 11 - Schematic cross-section of the rift valley showing pattern of normal faulting on inward- and outward-facing faults (upper panel; see Figure 9), with plots of seamount parameters versus age (lower panels). Circled numbers in upper panel relate to local fault pattern: (1) the relatively unfaulted inner rift-valley floor, (2) the lower walls of the rift valley where faults are predominantly inward-facing, (3) the upper rift-valley wall to the crest of the rift mountains, where inward-facing faults become inactive and outward-facing faults develop, (4) the ridge flank where there are no active faults. The lower panels show estimated seamount density (ν_{ot}); characteristic height (β^{-1}); height-to-diameter ratio (ξ_d); and plan-view aspect ratio (D_{max}/D_{min}), versus crustal age/distance from the ridge axis. Errors of one standard deviation about the estimated parameter are shown on the y-axis.

Figure 12 - Top: Three-dimensional perspective of DSL-120 bathymetry at Site B on ~24 Ma crust, illuminated from northeast. No vertical exaggeration. Note the three major east-dipping fault scarps that are heavily dissected by canyons, and the slide masses along the base of the central scarp. Strongly smoothed areas at the perimeter are regions for which there are no bathymetric data. Subtle horizontal "layering" along the central scarp is a data-processing artifact. Bottom: Similar view of DSL-120 bathymetry at Site A on ~11 Ma crust. East-dipping fault scarps are more numerous and smaller than at Site B, and crosscutting canyons are less well developed.

Figure 13 - DSL-120 sidescan-sonar images of fault scarps (strong backscatter is dark) at Sites B, A, and D within the Acoustic Reverberation Corridor. Top: East-dipping central scarp at Site B (see the upper panel of Figure 12) centered at 26°34.3'N, 48°04.6'W. The scarp is extensively dissected into a trellis pattern of cross-scarp canyons and intersecting scarp-parallel gullies. Center: East-dipping scarp at eastern edge of Site A (see the lower panel of Figure 12) centered at 26°07.8'N, 46°12.2'W. A nascent trellis drainage pattern is observed. Bottom: South-southeast-dipping scarp at

Site D (~4 Ma crust) centered at 26°05.0'N, 45°15.8'W. Faults around displaced blocks probably will develop into cross-scarp canyons over time. Small scarp-parallel faults are visible but have not developed into gullies to form a trellis drainage pattern.

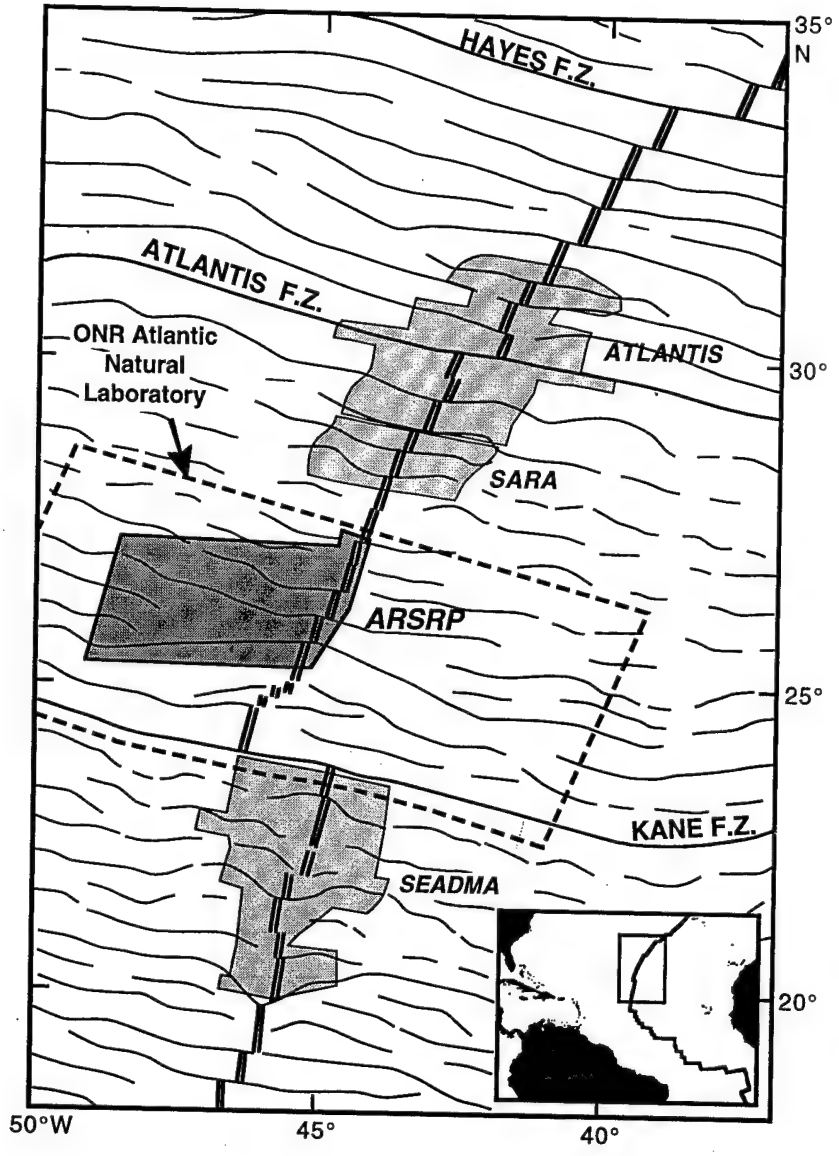
HAYES F.Z.
35°
N
ATLANTIS F.Z.
ONR Atlantic
Natural
Laboratory
ATLANTIS
30°
SARA
ARSRP
25°
KANE F.Z.
SEADMA
20°
50°W
45°
40°

Figure 1

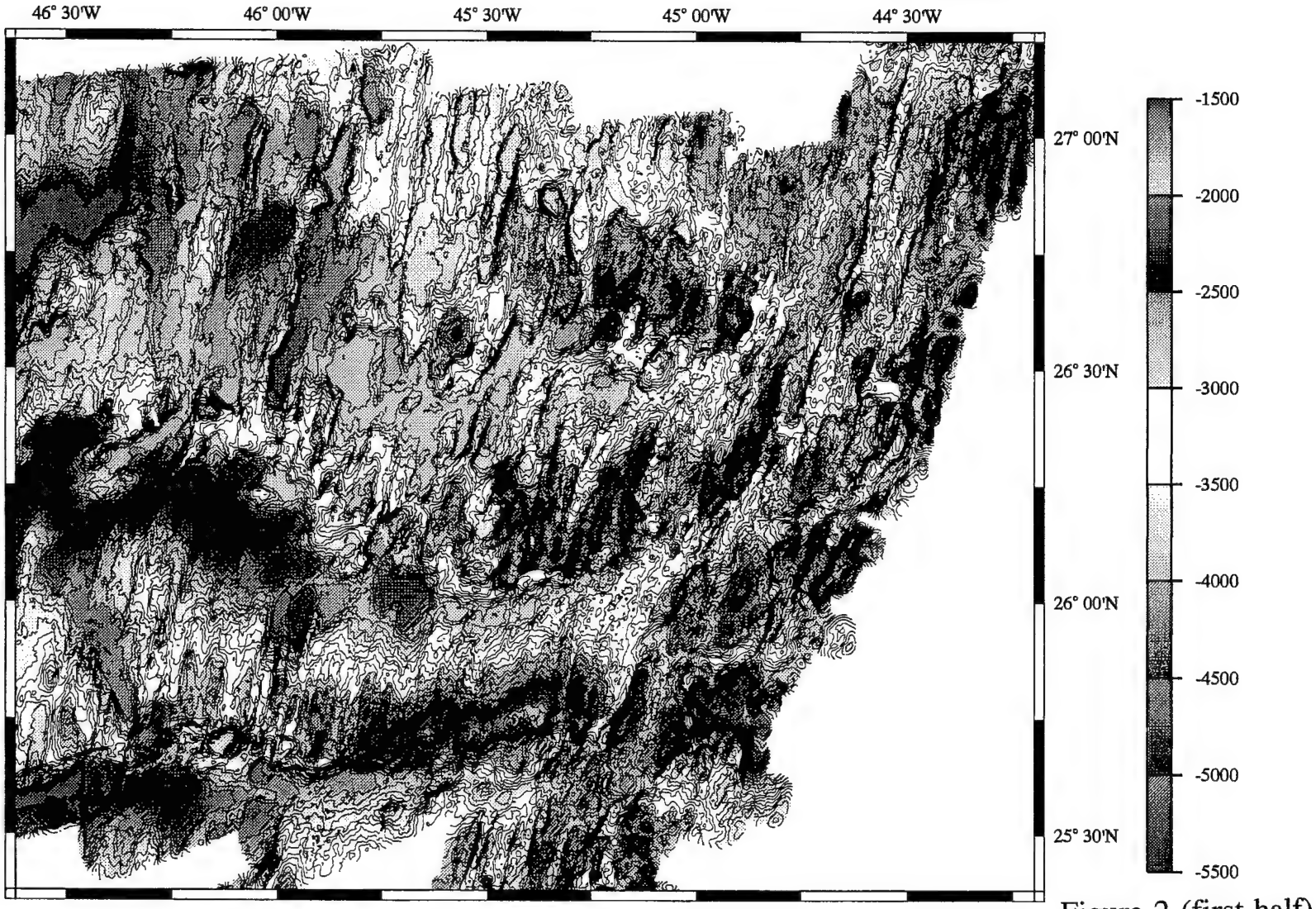

Figure 2 (first half)

Figure 2

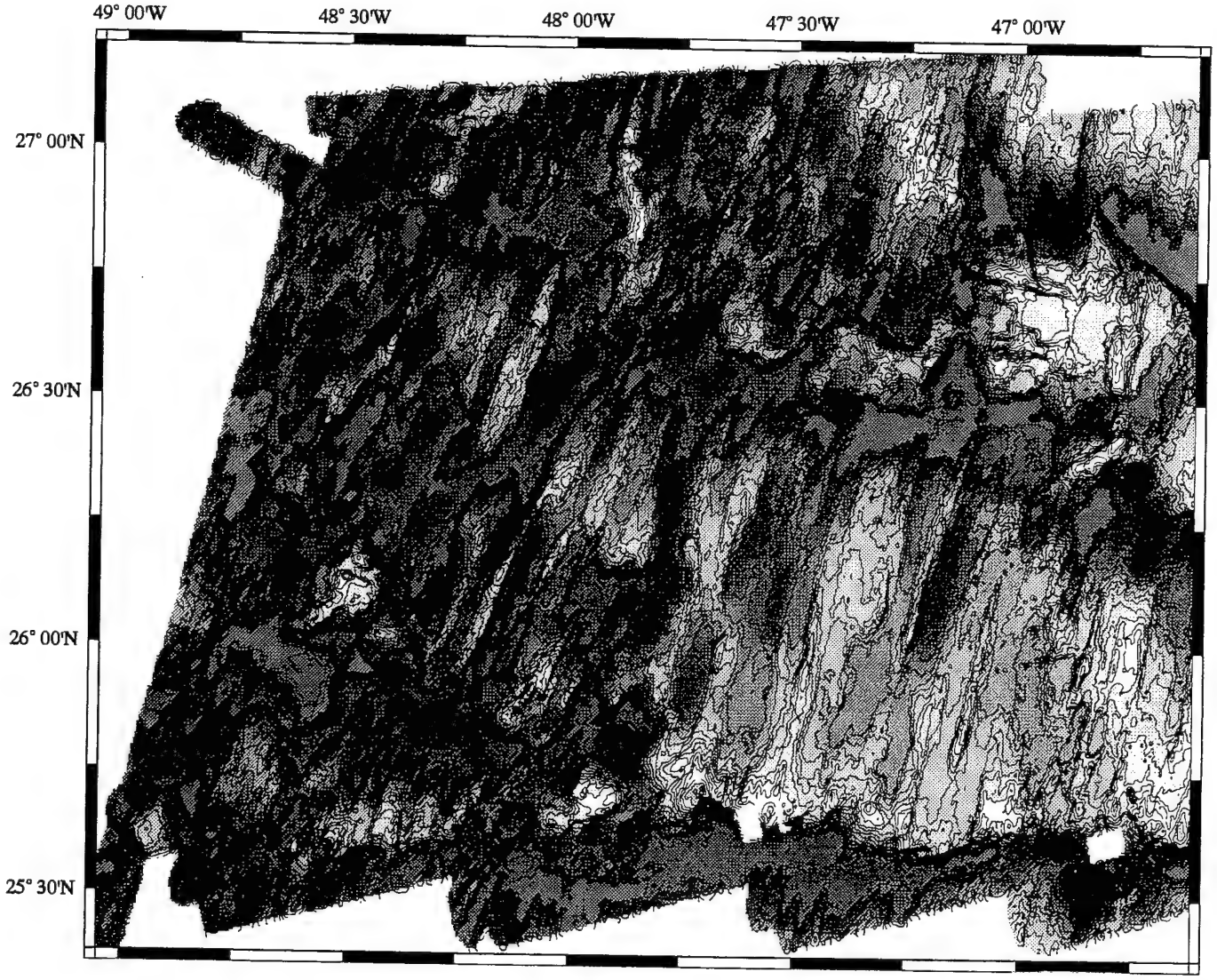

Figure 2 (second half)

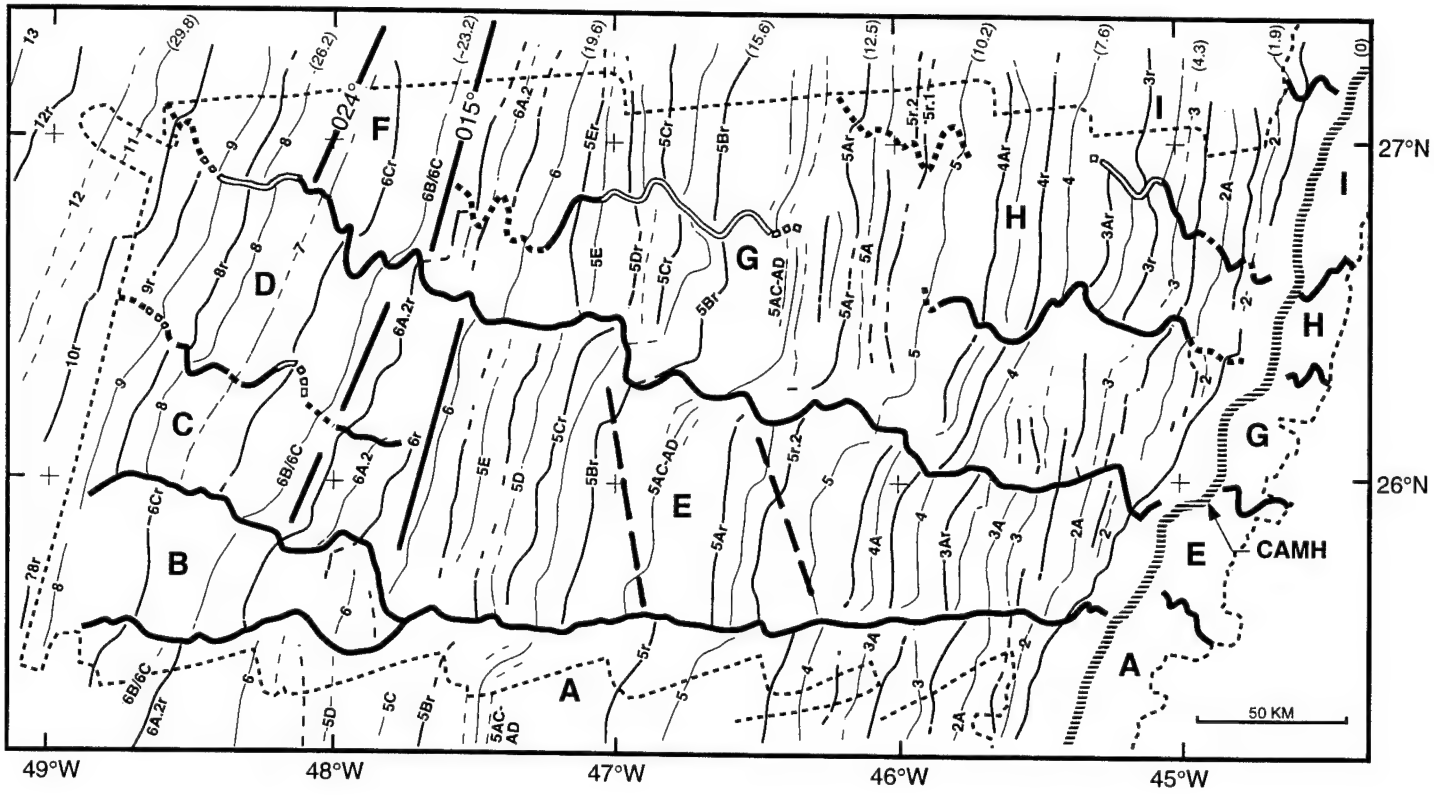

Figure 3

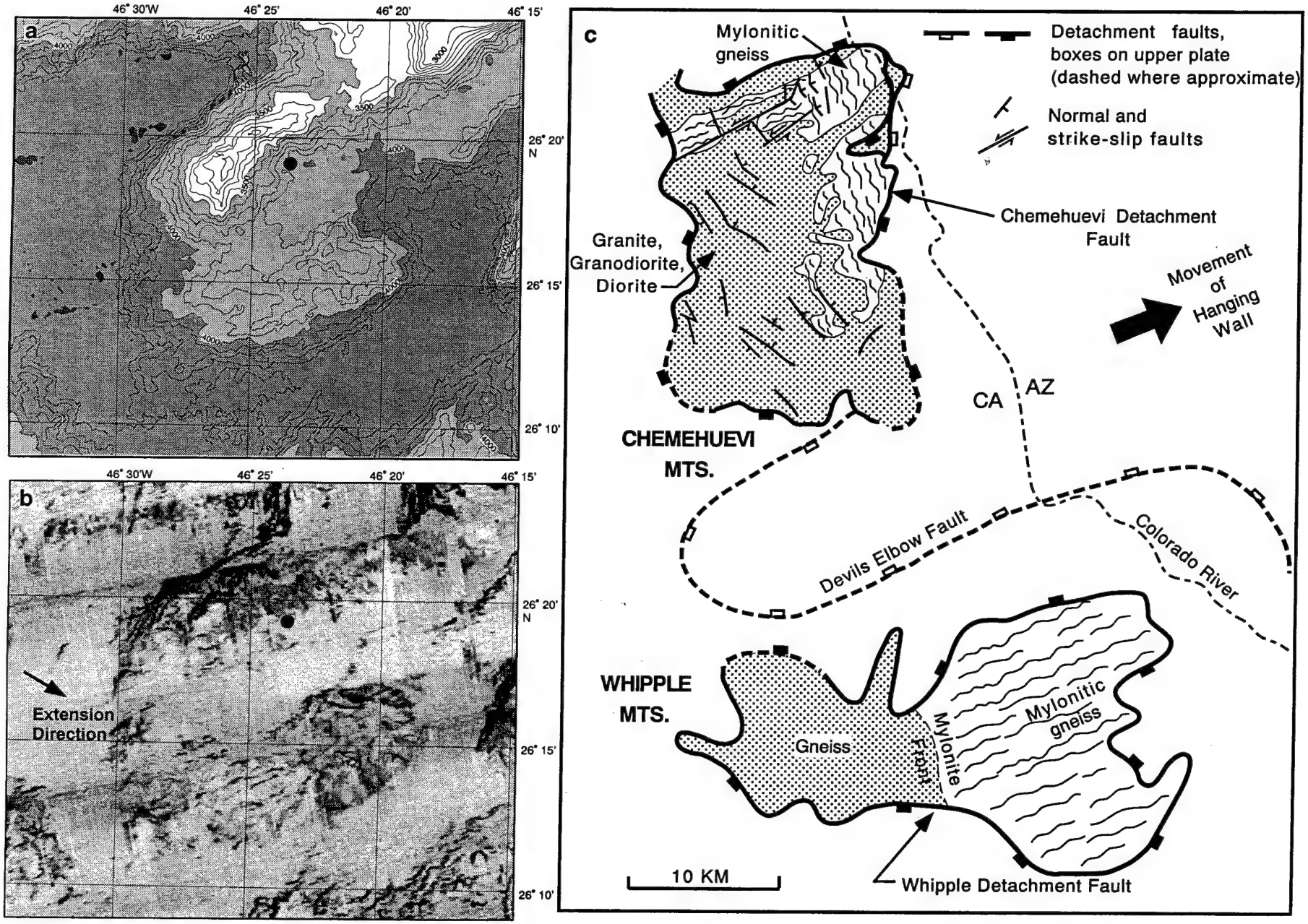
a
46° 30'W
46° 25'
46° 20'
46° 15'
26° 20' N
26° 15'
26° 10'
b
Extension Direction
c
Mylonitic gneiss
Detachment faults, boxes on upper plate (dashed where approximate)
Normal and strike-slip faults
Chemehuevi Detachment Fault
Granite, Granodiorite, Diorite
Movement of Hanging Wall
CA
AZ
CHEMEHUEVI MTS.
Devils Elbow Fault
Colorado River
WHIPPLE MTS.
Gneiss
Mylonite Front
Mylonitic gneiss
10 KM
Whipple Detachment Fault

Figure 4

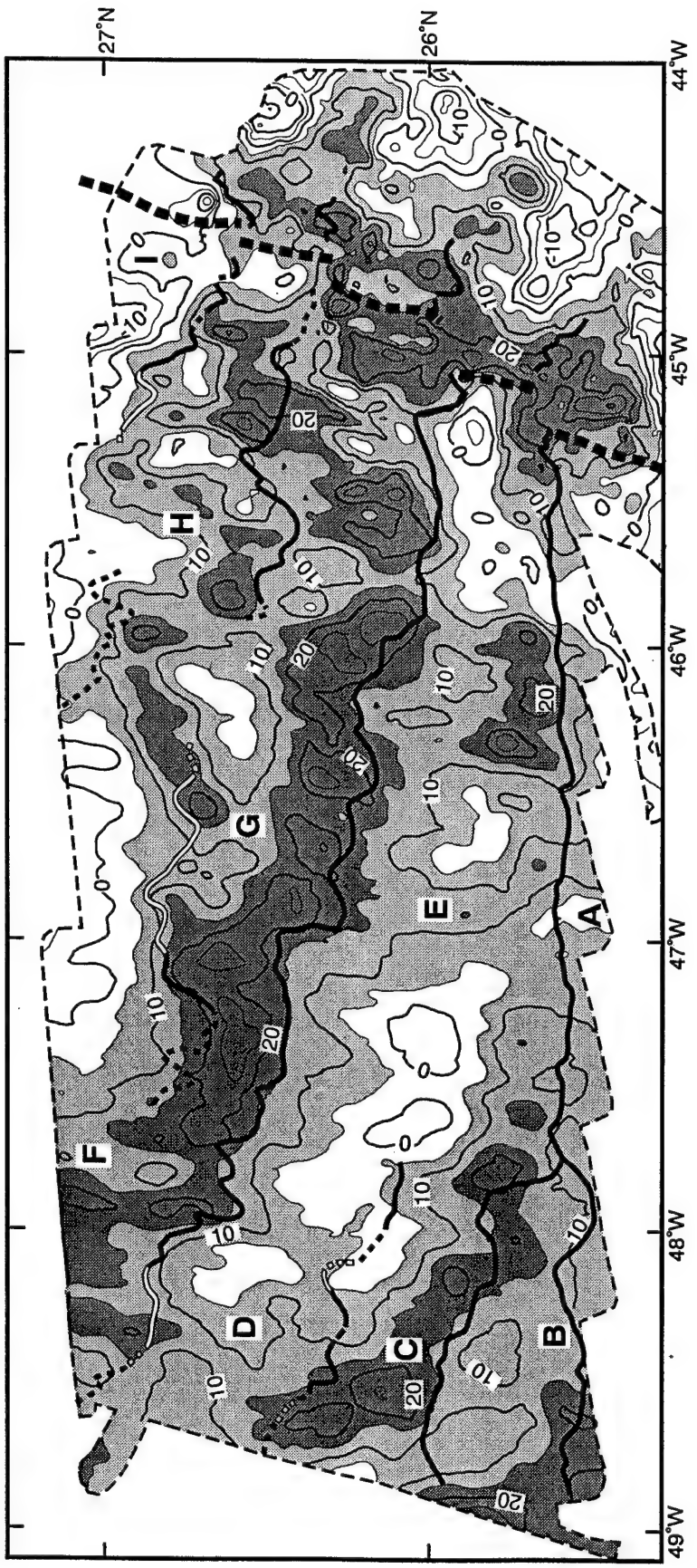

Figure 5

Figure 6

Sediment Thickness Maps
(Six foldouts)

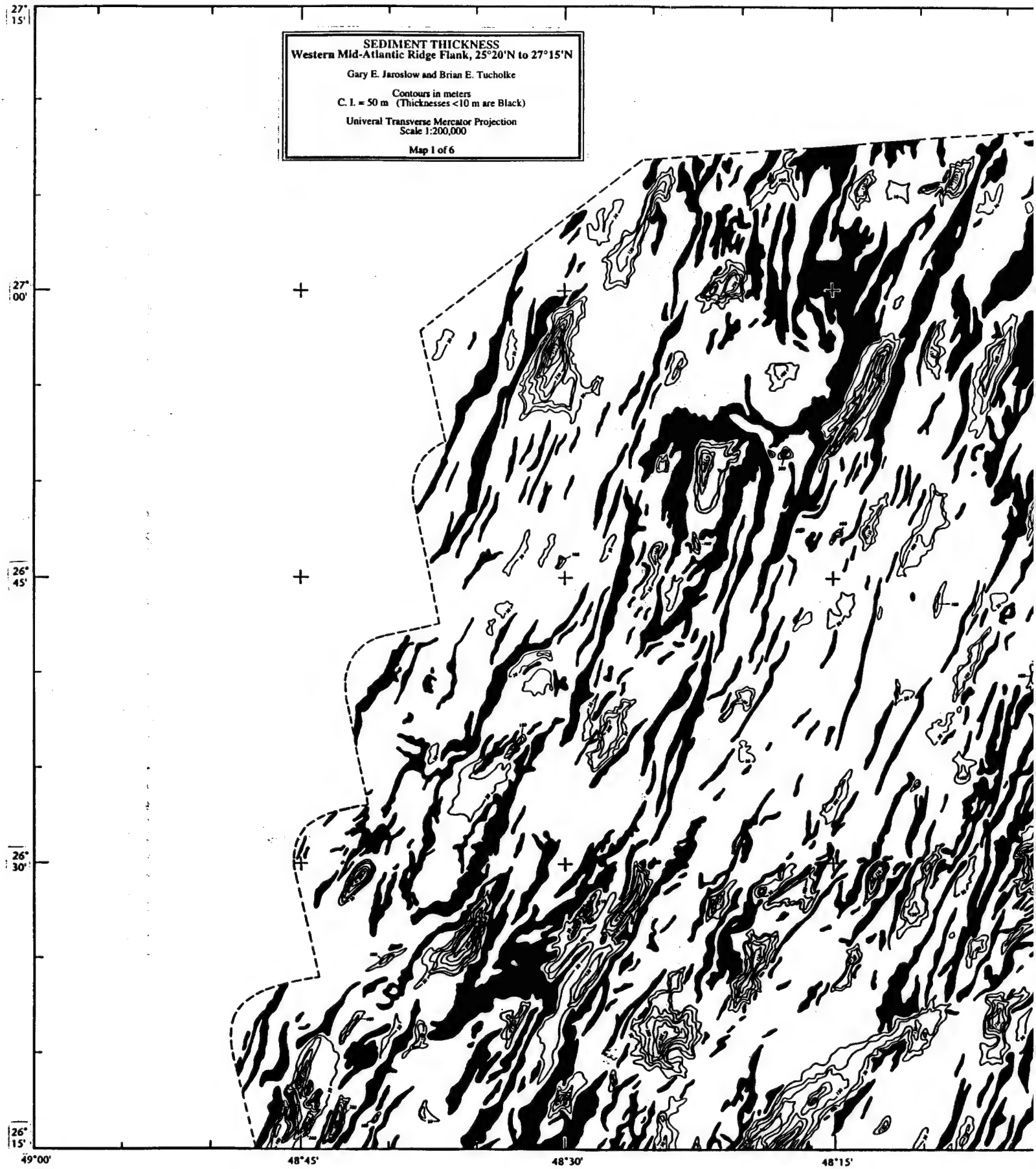
49°00'
48°45'
48°30'
48°15'
27° 15'
27° 00'
26° 45'
26° 30'
26° 15'
SEDIMENT THICKNESS
Western Mid-Atlantic Ridge Flank, 25°20'N to 27°15'N
Gary E. Jaroslow and Brian E. Tucholke
Contours in meters
C. I. = 50 m (Thicknesses <10 m are Black)
Univeral Transverse Mercator Projection
Scale 1:200,000
Map 1 of 6


48°15'
48°00'
47°45'
47°30'
27° 15'
27° 00'
26° 45'
26° 30'
26° 15'


47°30'
47°00'
27° 15'
27° 00'
26° 45'
26° 30'
26° 15'
47°30'
47°00'
SEDIMENT THICKNESS
Western Mid-Atlantic Ridge Flank, 25°20'N to 27°15'N
Gary E. Jaroslow and Brian E. Tucholke
Contours in meters
C. I. = 50 m (Thicknesses <10 m are Black)
Univeral Transverse Mercator Projection
Scale 1:200,000
Map 2 of 6


SEDIMENT THICKNESS
Western Mid-Atlantic Ridge Flank, 25°20'N to 27°15'N
Gary E. Jaroslow and Brian E. Tucholke
Contours in meters
C. I. = 50 m (Thicknesses <10 m are Black)
Univeral Transverse Mercator Projection
Scale 1:200,000
Map 2 of 6
46°30'
46°00'
27° 15'
27° 00'
26° 45'
26° 30'
26° 15'

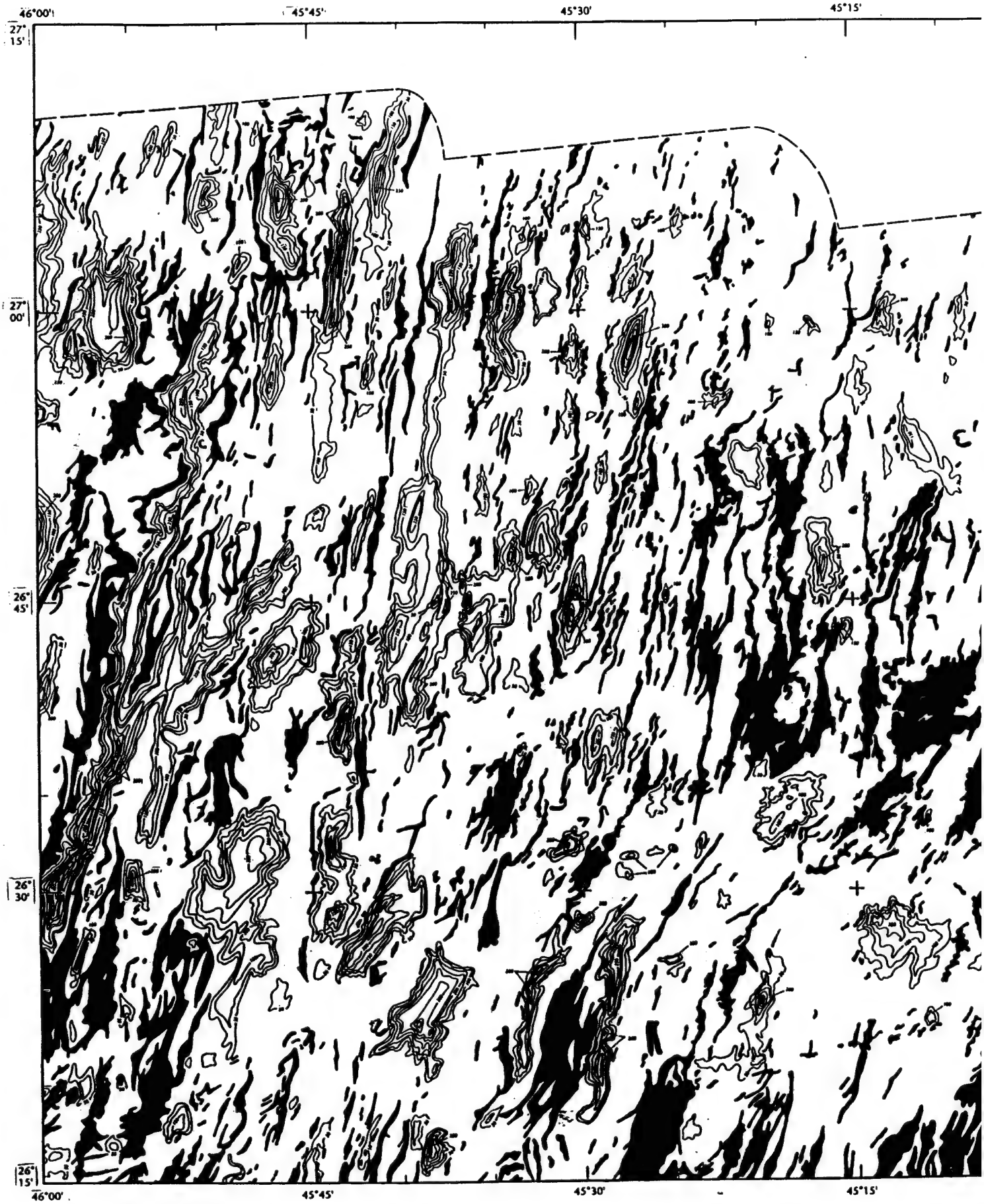
46°00'
45°45'
45°30'
45°15'
27° 15'
27° 00'
26° 45'
26° 30'
26° 15'

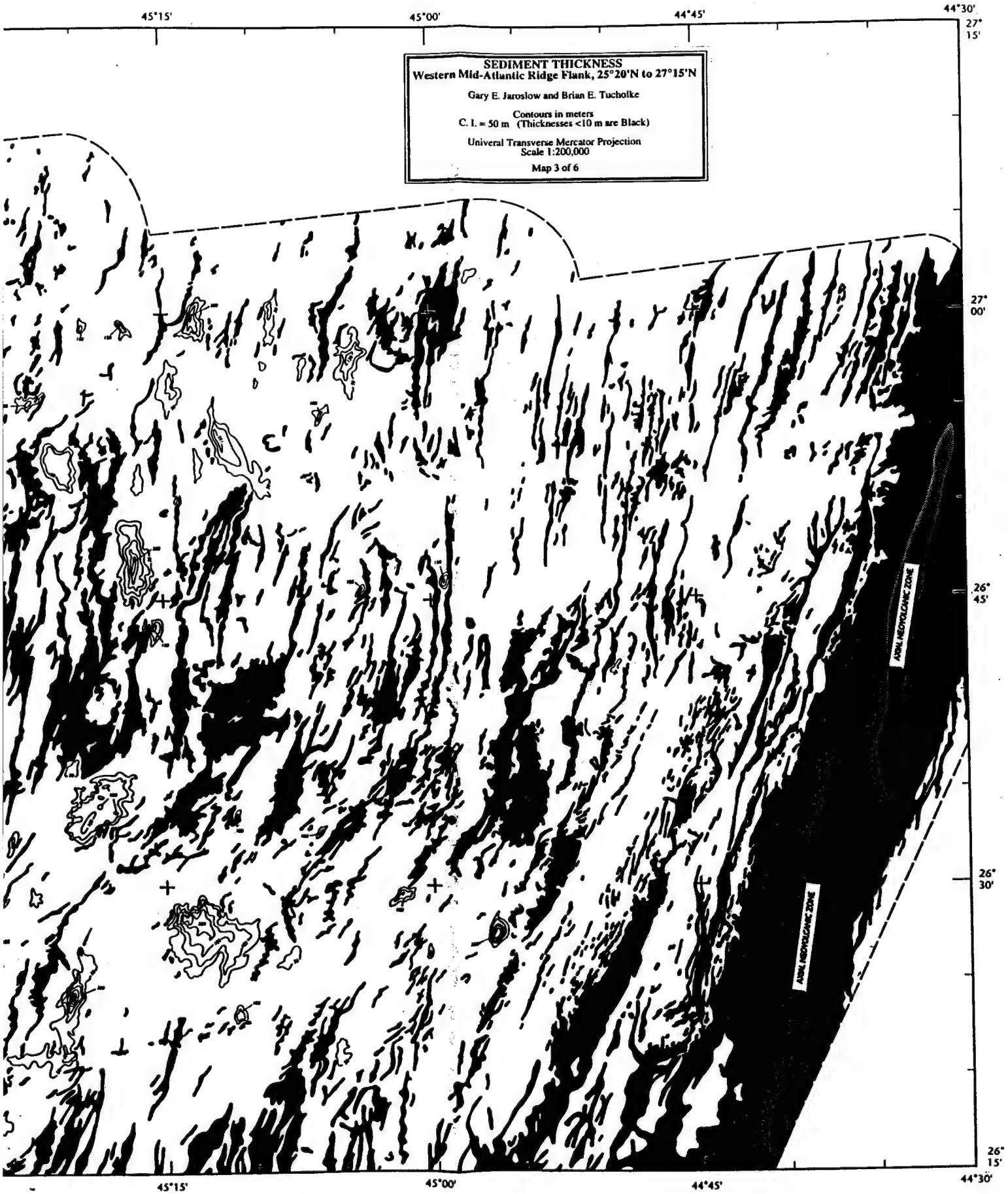
SEDIMENT THICKNESS
Western Mid-Atlantic Ridge Flank, 25°20'N to 27°15'N
Gary E. Jaroslow and Brian E. Tucholke
Contours in meters
C. I. = 50 m (Thicknesses <10 m are Black)
Univeral Transverse Mercator Projection
Scale 1:200,000
Map 3 of 6
45°15'
45°00'
44°45'
44°30'
27° 15'
27° 00'
26° 45'
26° 30'
26° 15'
AXIAL NEOVOLCANIC ZONE
AXIAL NEOVOLCANIC ZONE

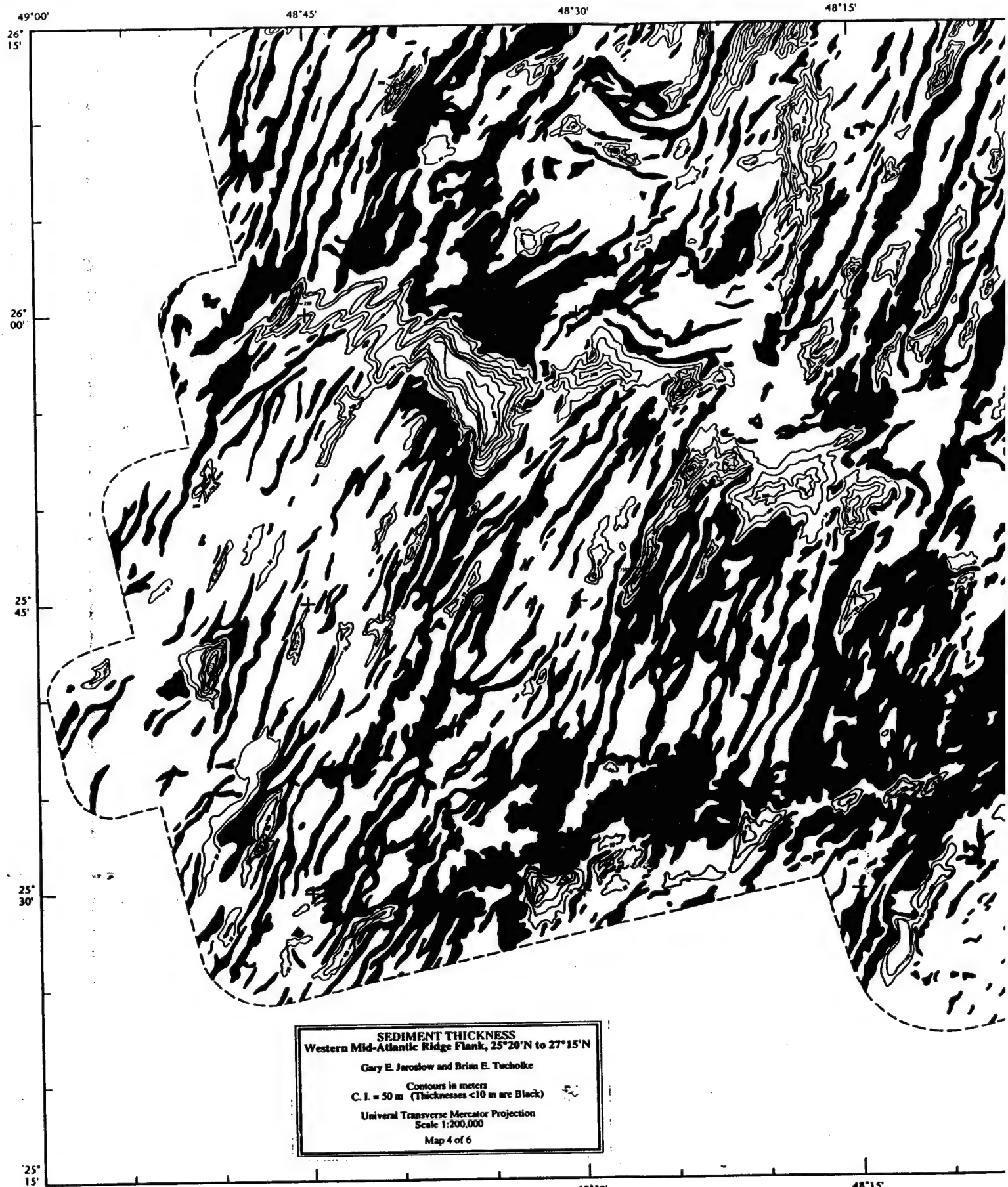

SEDIMENT THICKNESS
Western Mid-Atlantic Ridge Flank, 25°20'N to 27°15'N

Gary E. Jaroslow and Brian E. Tucholke

Contours in meters
C. I. = 50 m (Thicknesses <10 m are Black)

Univeral Transverse Mercator Projection
Scale 1:200,000

Map 4 of 6


48°15'
48°00'
47°45'
47°30'
26° 15'
26° 00'
25° 45'
25° 30'
25° 15'

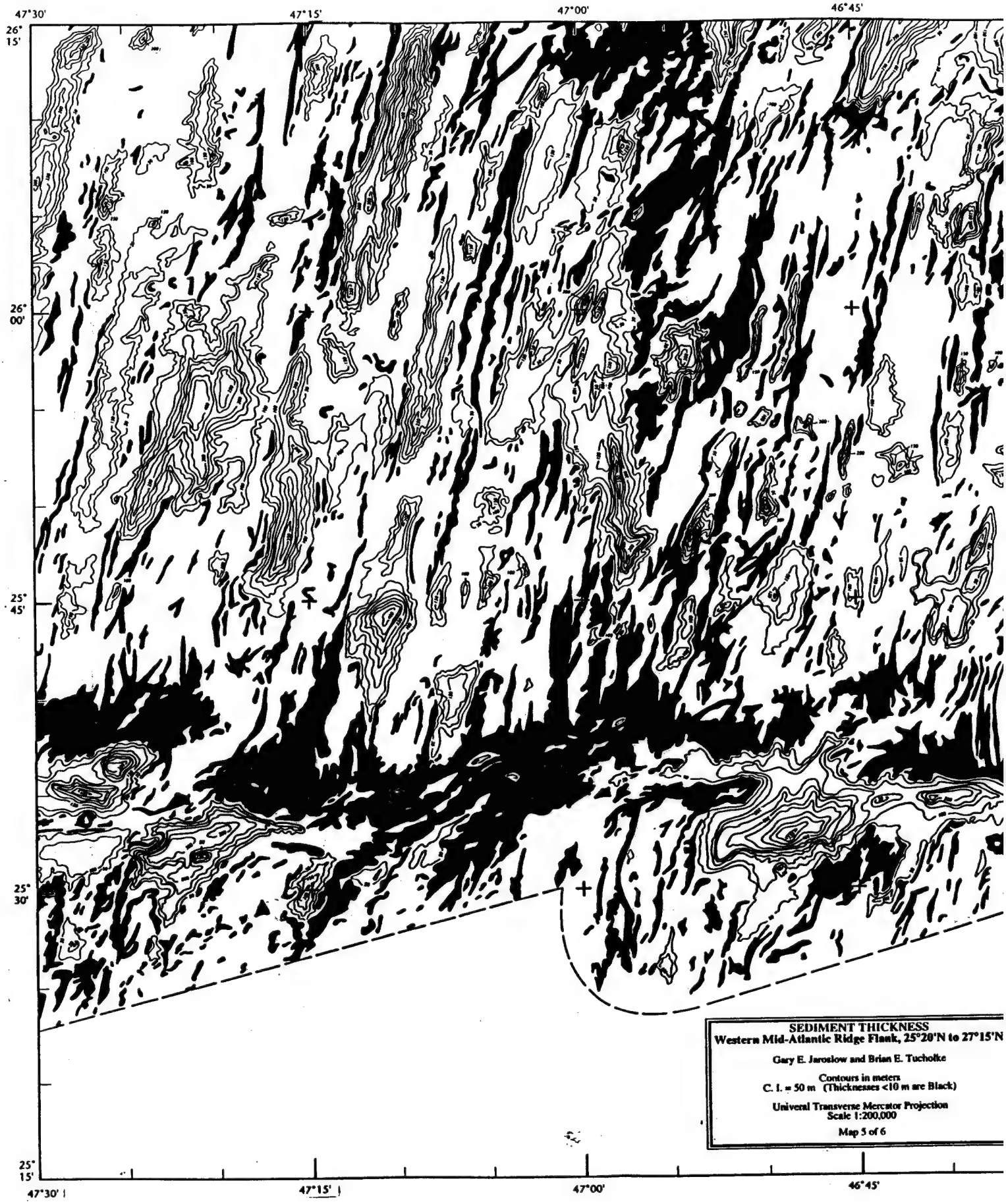
47°30'
47°15'
47°00'
46°45'
26° 15'
26° 00'
25° 45'
25° 30'
25° 15'
SEDIMENT THICKNESS
Western Mid-Atlantic Ridge Flank, 25°20'N to 27°15'N
Gary E. Jaroslow and Brian E. Tucholke
Contours in meters
C. I. = 50 m (Thicknesses <10 m are Black)
Univeral Transverse Mercator Projection
Scale 1:200,000
Map 5 of 6

SEDIMENT THICKNESS
Western Mid-Atlantic Ridge Flank, 25°20'N to 27°15'N

Gary E. Jaroslow and Brian E. Tucholke

Contours in meters
C. I. = 50 m (Thicknesses <10 m are Black)

Univeral Transverse Mercator Projection
Scale 1:200,000

Map 5 of 6

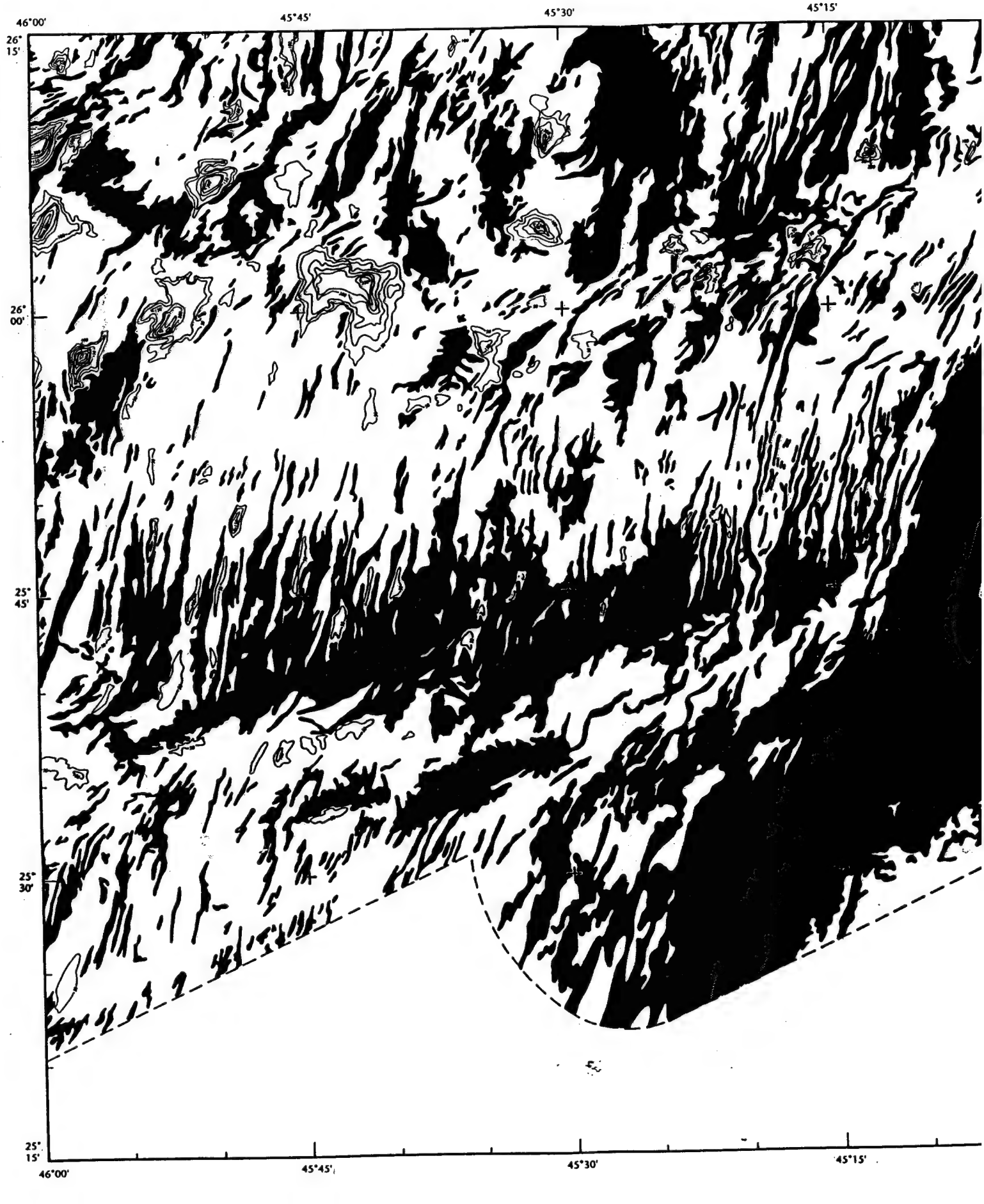
46°00'
45°45'
45°30'
45°15'
26° 15'
26° 00'
25° 45'
25° 30'
25° 15'

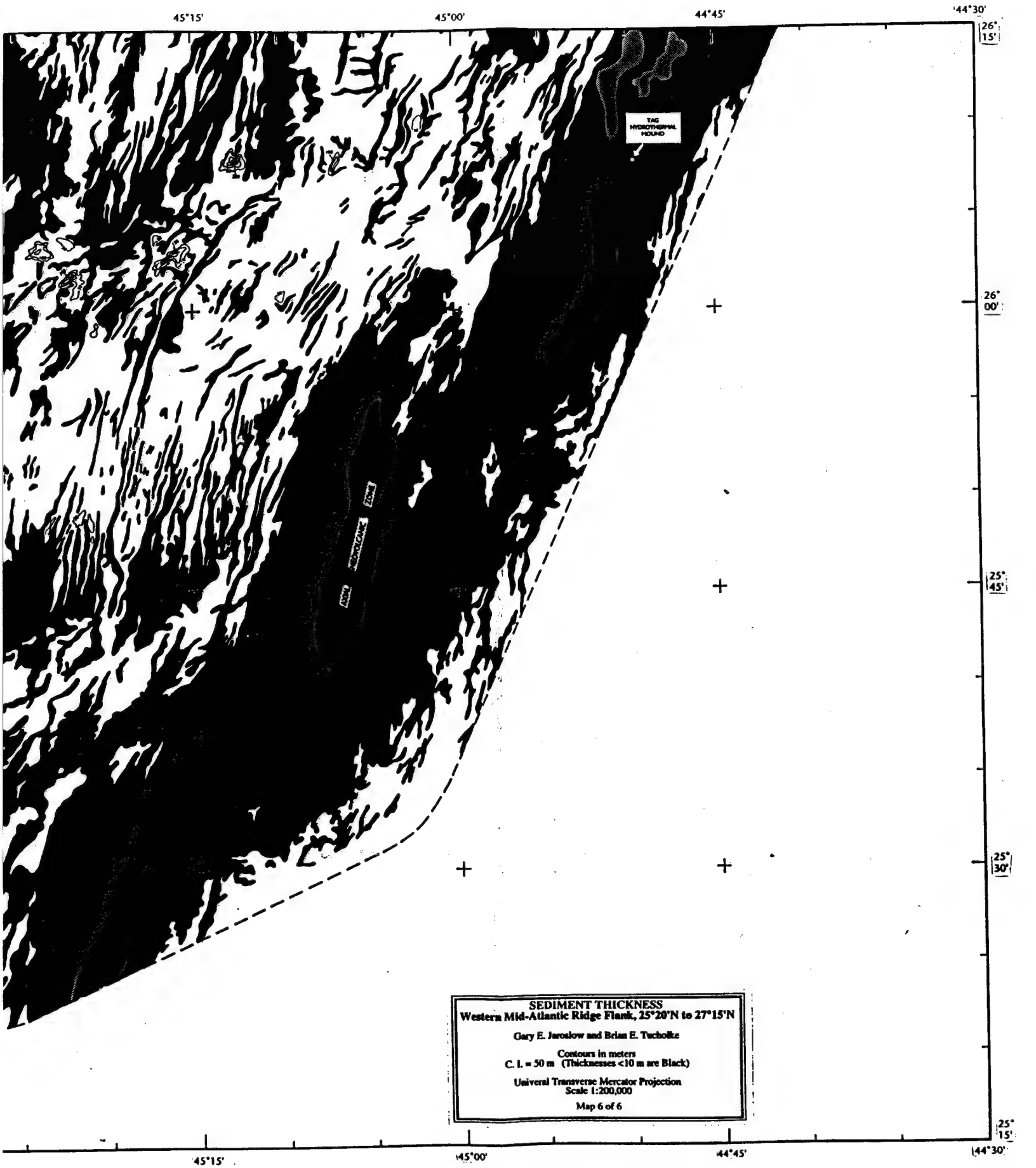
45°15'
45°00'
44°45'
44°30'
26° 15'
26° 00'
25° 45'
25° 30'
25° 15'
TAG HYDROTHERMAL MOUND
FOX
KANE FRACTURE ZONE
SEDIMENT THICKNESS
Western Mid-Atlantic Ridge Flank, 25°20'N to 27°15'N
Gary E. Jaroslow and Brian E. Tucholke
Contours in meters
C. I. = 50 m (Thicknesses <10 m are Black)
Univeral Transverse Mercator Projection
Scale 1:200,000
Map 6 of 6

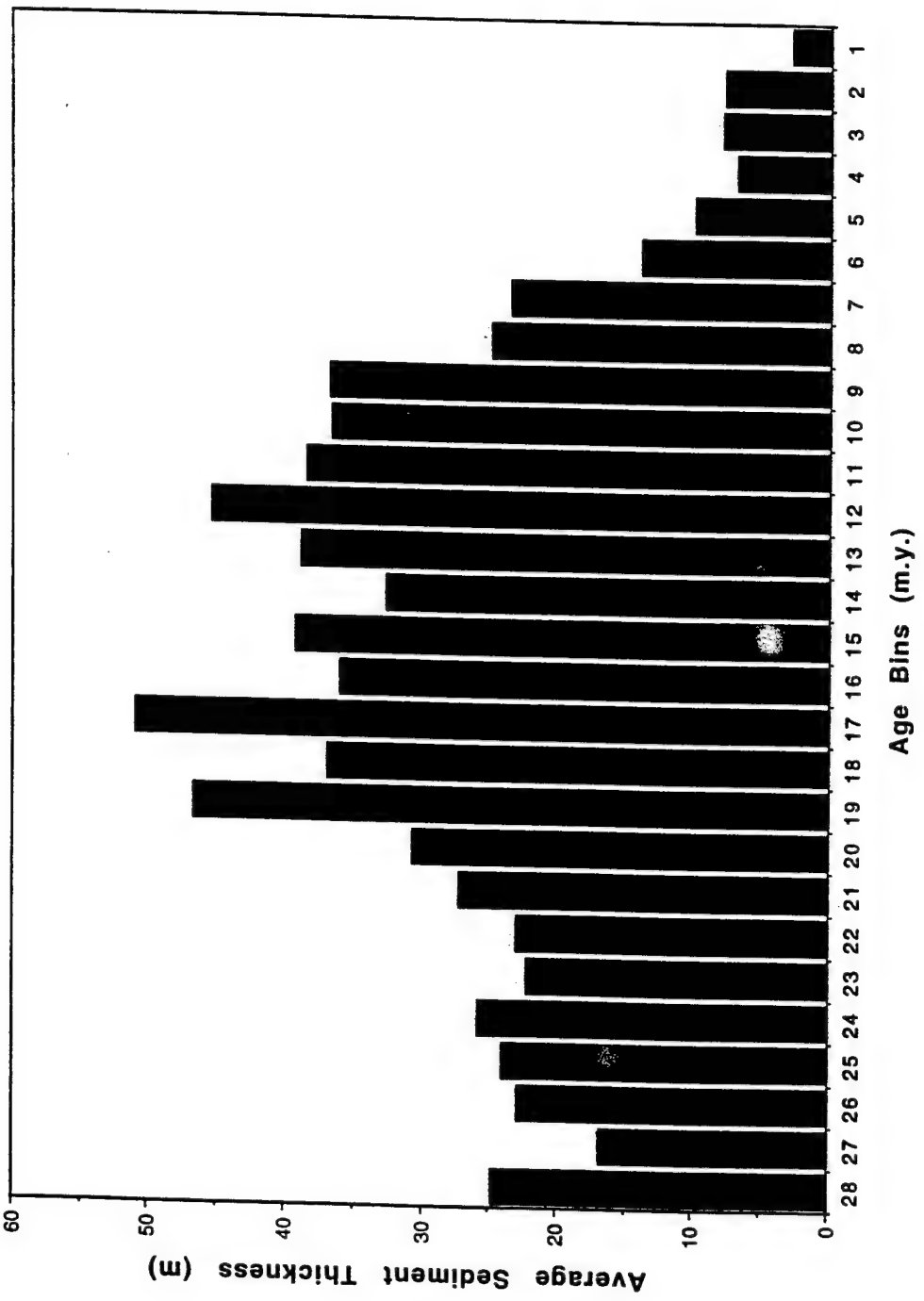
Average Sedimentary Thickness (m)
0
10
20
30
40
50
60
Age Bins (m.y.)
28 27 26 25 24 23 22 21 20 19 18 17 16 15 14 13 12 11 10 9 8 7 6 5 4 3 2 1

Figure 7

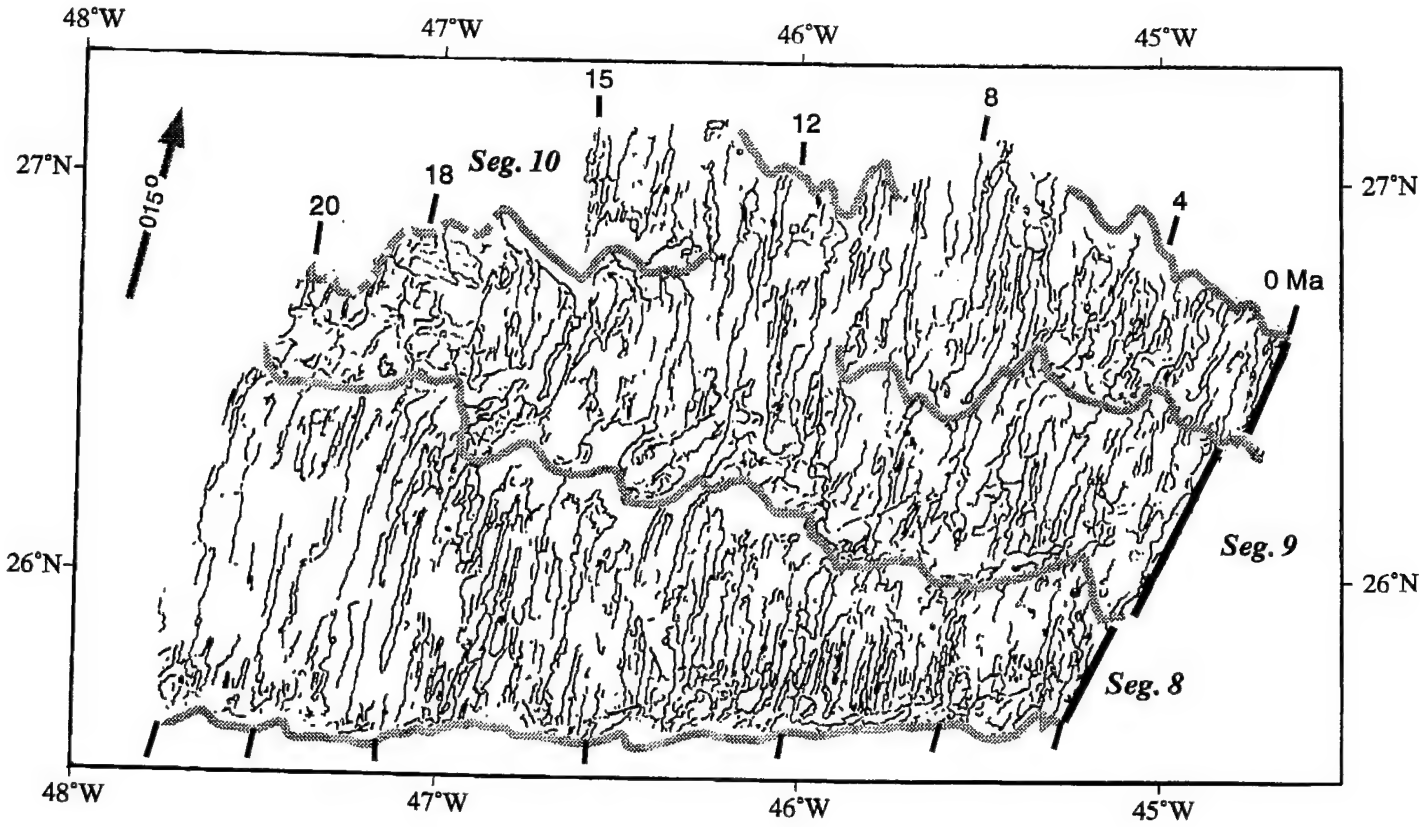

Figure 8

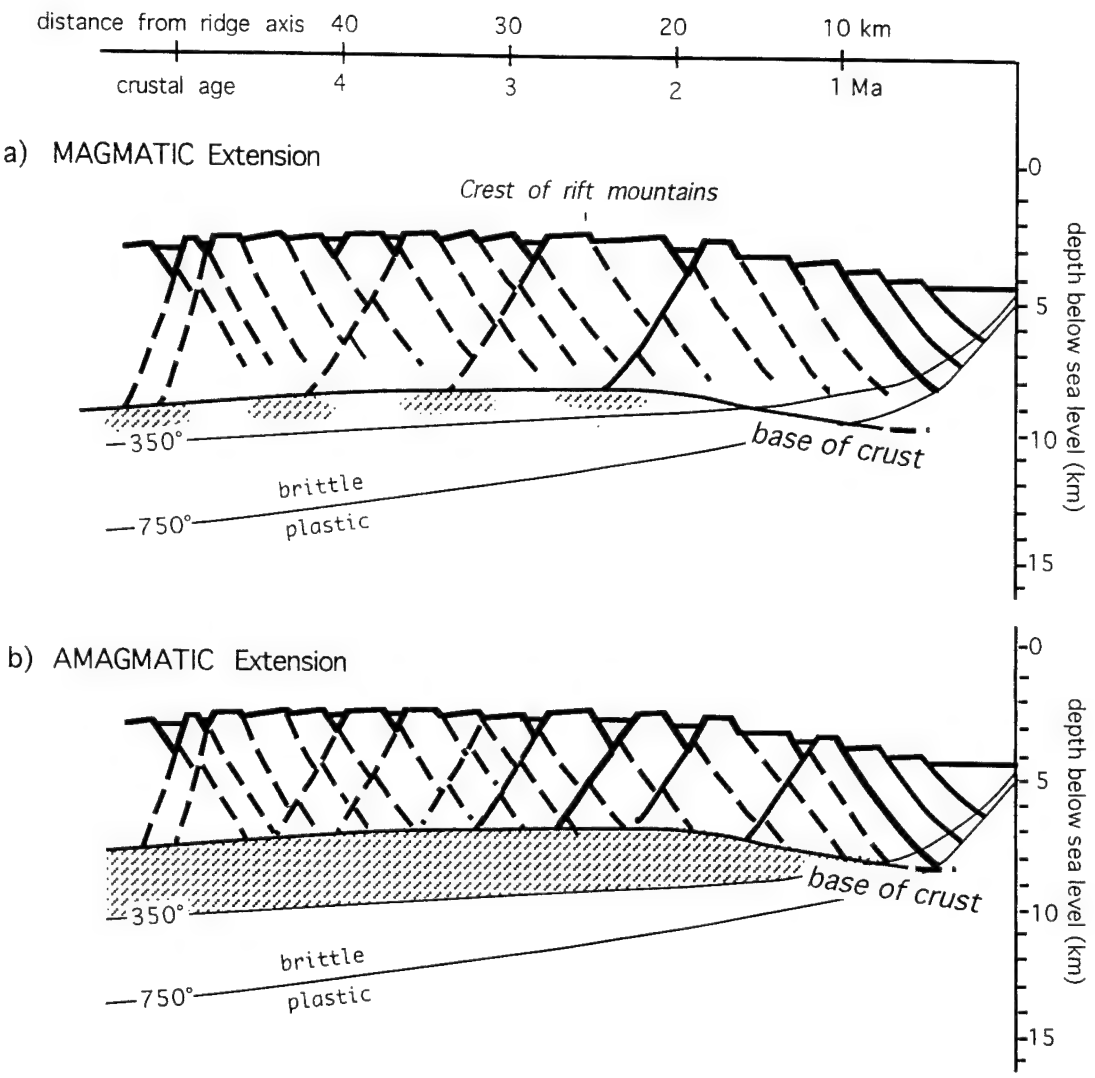
distance from ridge axis 40 30 20 10 km
crustal age 4 3 2 1 Ma
a) MAGMATIC Extension
Crest of rift mountains
0
5
10
15
depth below sea level (km)
350°
750°
brittle
plastic
base of crust
b) AMAGMATIC Extension
0
5
10
15
depth below sea level (km)
350°
750°
brittle
plastic
base of crust

Figure 9

MID-ATLANTIC RIDGE SEAMOUNTS, 26°N

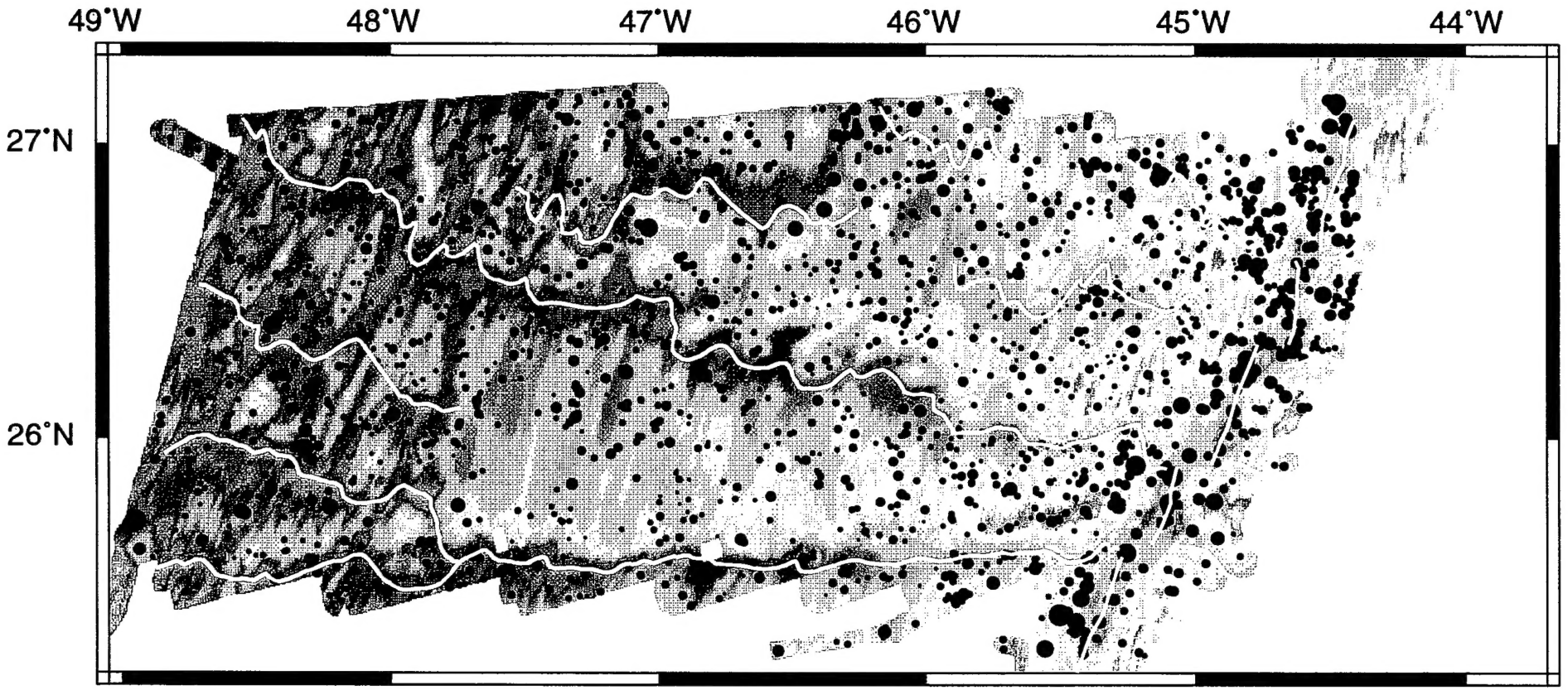

Figure 10

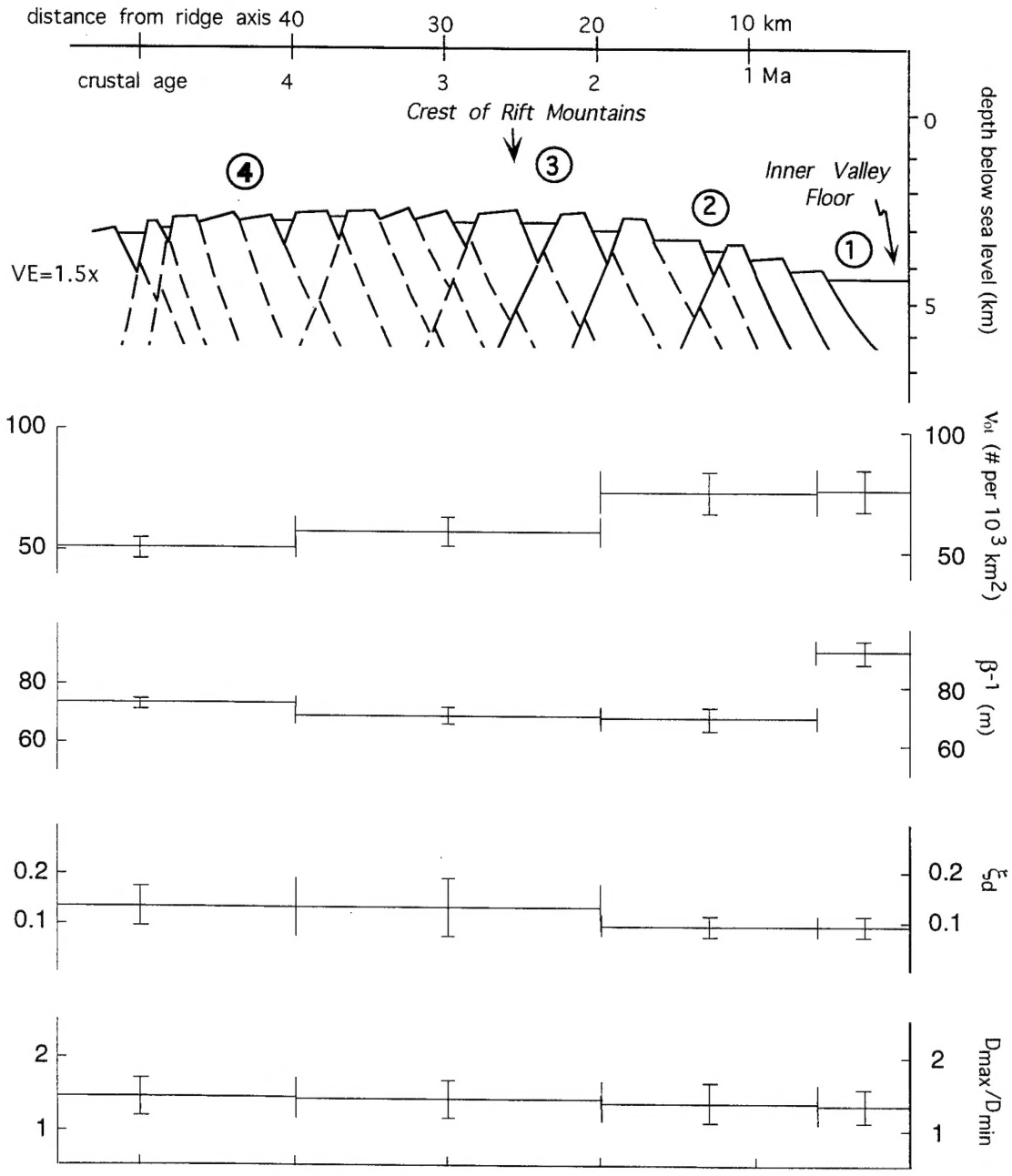
distance from ridge axis 40
30
20
10 km
crustal age
4
3
2
1 Ma
Crest of Rift Mountains
Inner Valley Floor
VE=1.5x
depth below sea level (km)
0
5
100
50
V_{0l} (# per 10^3 km^2)
80
60
β^{-1} (m)
0.2
0.1
ξ_d
2
1
D_{max}/D_{min}

Figure 11

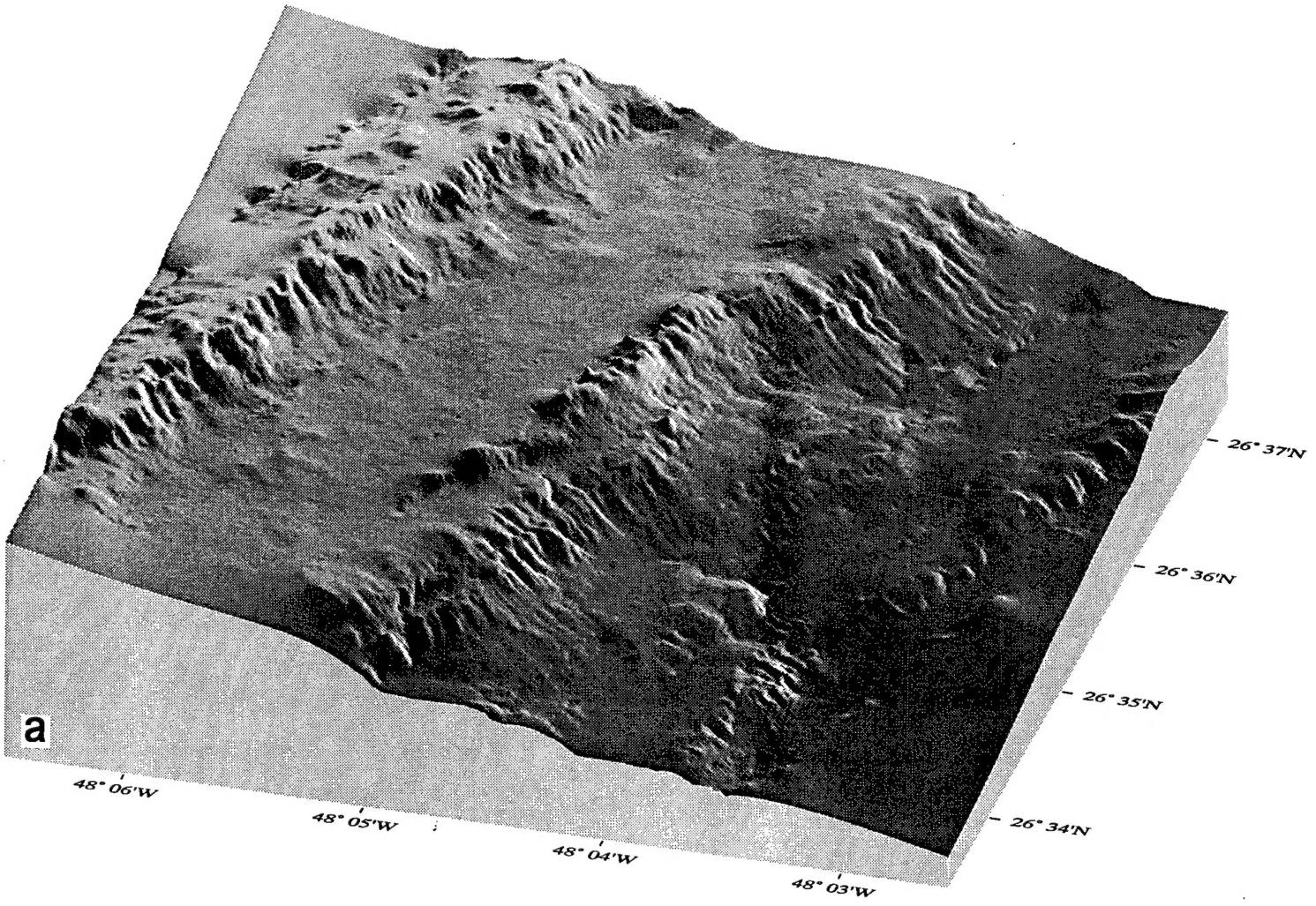
a
48° 06'W
48° 05'W
48° 04'W
48° 03'W
26° 37'N
26° 36'N
26° 35'N
26° 34'N

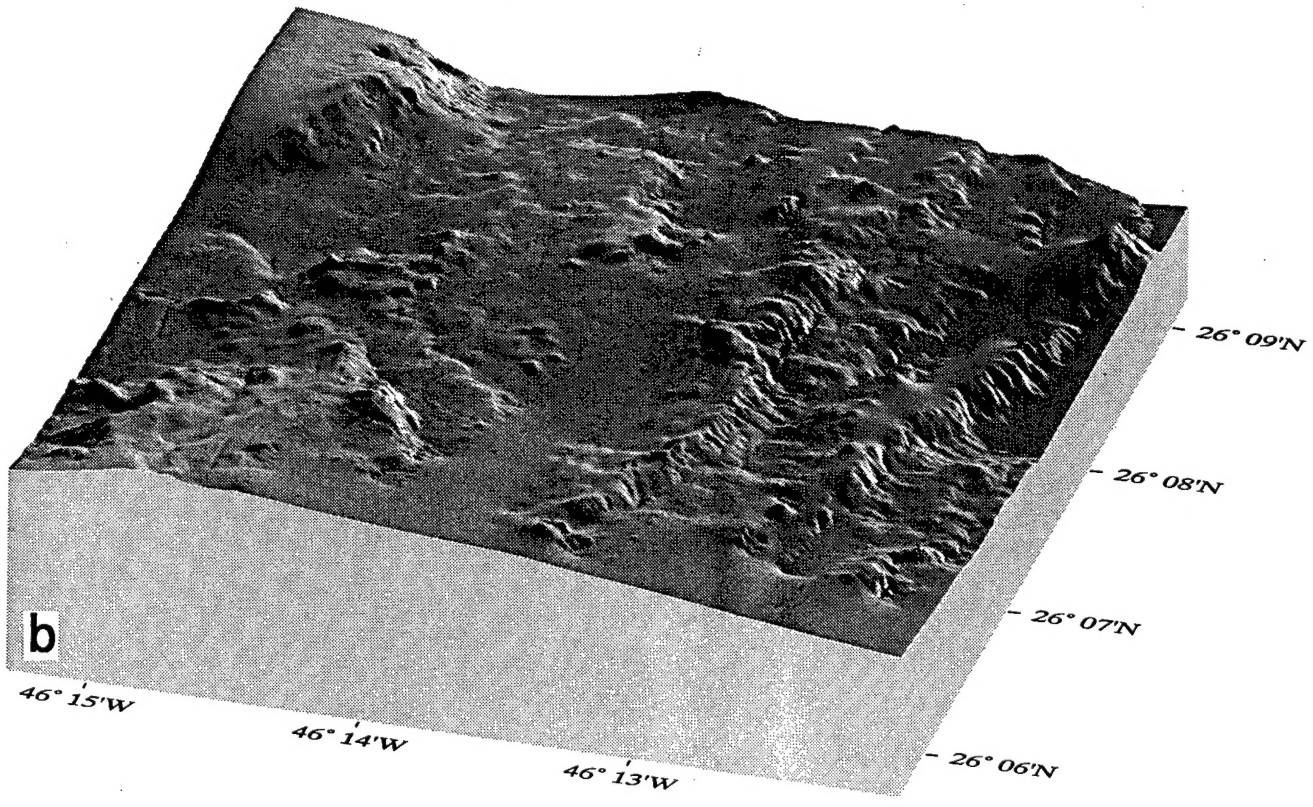
b
46° 15'W
46° 14'W
46° 13'W
26° 09'N
26° 08'N
26° 07'N
26° 06'N

Figure 12

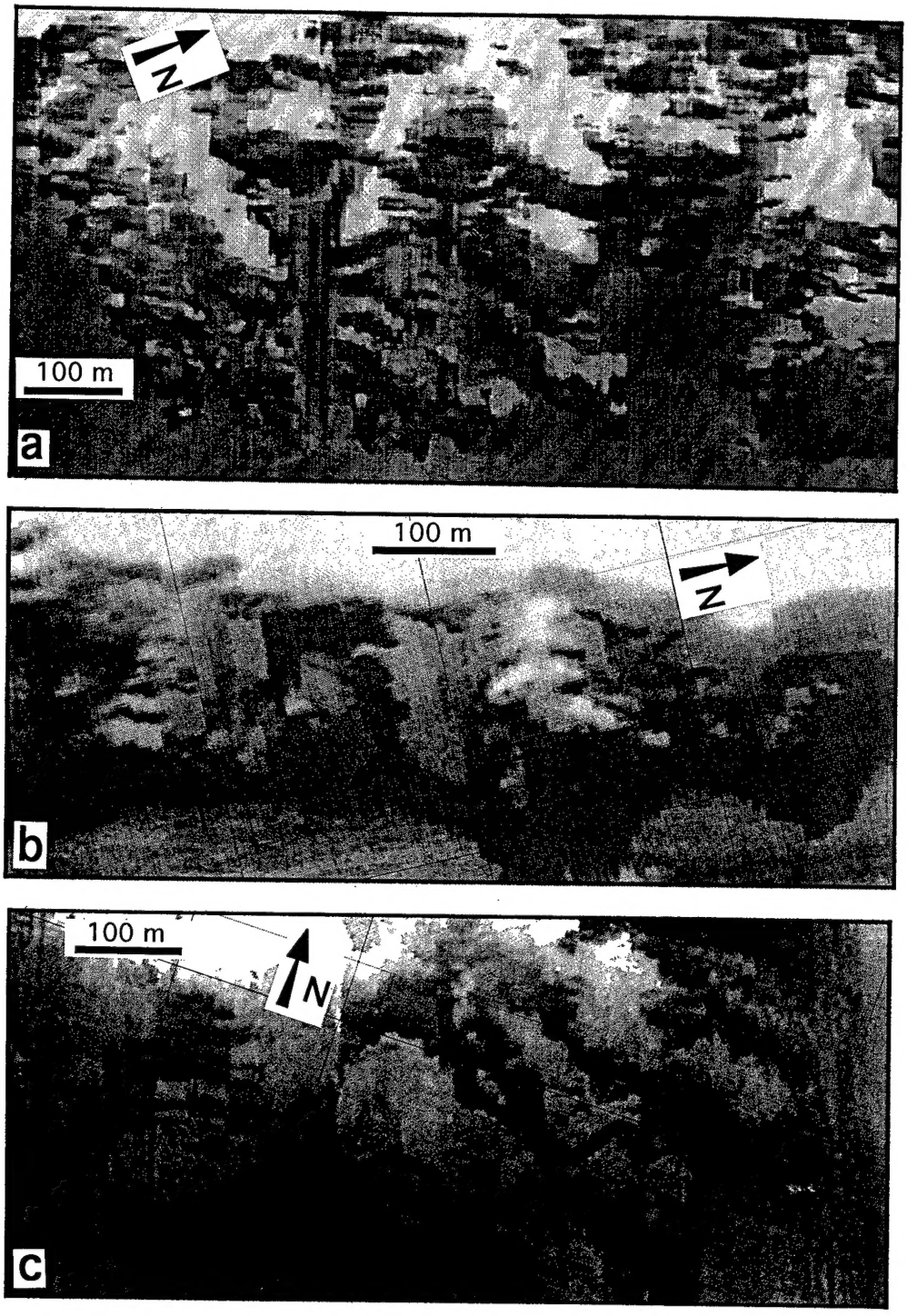

Figure 13